Report Title:

Development of Pd-Ag Composite Membrane for Separation of Hydrogen at Elevated Temperature

Report Type: Final Technical Report

Reporting Period Start Date: 09/01/2005 End Date: 02/28/2009

Principal Author(s): Shamsuddin Ilias

Report Issue Date: November 5, 2009 DOE Award No.: DE-FG26-05NT42492

Name and Address of Submitting Organization:

North Carolina A&T State University
Department of Chemical and Bioengineering
Greensboro, NC 27411
E-mail: ilias@ncat.edu
Tel: (336) 334-7564 ext 317 Fax: (336) 334-7417

DISCLAIMER

ABSTRACT

Pd-based membrane reactor offers the possibility of combining reaction and separation in a single operation at high temperatures to overcome the equilibrium limitations experienced in conventional reactor configurations. In this project to develop a defect-free and thermally-stable Pd-film on microporous stainless steel (MPSS) support for H_2-separation and membrane reactor applications, the electroless plating process was revisited with an aim to improve the membrane morphology. Specifically, this study includes; (a) an improvement of activation step using Pulse Laser Deposition (PLD), (b) development of a novel surfactant induced electroless plating (SIEP) for depositing robust Pd-film on microporous support, and (c) application of Pd-membrane as membrane reactor in steam methanol reforming (SMR) reactions.

In conventional sensitization/activation steps, Pd-seed deposition is uneven and penetration in the pore is problematic. To address this, PLD developed Pd-nuclei directly onto microporous substrate was explored. EDX (Energy Dispersive X-ray) and SEM (Scanning Electron Microscopy) results showed significant improved in Pd-nuclei deposition.

In electroless plating, it was identified that the gas bubbles (ammonia and nitrogen) that released due to autocatalytic reactions tend to adhere to the substrate surface and result in poor Pd-deposition. Incorporation of cationic surface active agents with favorable structures into the plating bath appears to be a promising remedy of surface to prevent gas bubbles from growing within the vicinity of the plating substrate. More importantly, suitable cationic charge and concentration would be useful to tailor the Pd-grain size and subsequent agglomeration. The surface morphology and compositional microstructures were examined using SEM coupled with in-situ EDS (Energy Dispersive Spectroscopy).

Steam methanol reforming (SMR) was carried out in a Pd-MPSS membrane reactor fabricated by SIEP method. Experimental results along with modeling work revealed that the Pd-based membrane reactor was superior to conventional non-membrane reforming reactors with respect to conversion, selectivity and hydrogen productivity.

In summary, we demonstrated that by using suitable surfactant in electroless plating, the Pd-film morphology can be significantly improved. This is a significant development in electroless plating method. This work resulted in an US patent filing. The Pd-MPSS membrane fabricated by SIEP showed excellent H_2-permselectivity. The application of Pd-MPSS membrane as membrane reactor-separator is demonstrated by running SMR reaction.

TABLE OF CONTENTS

Title Page i

Disclaimer ii

Abstract iii

Table of Contents iv

Introduction 1

Research Objectives 2

Fabrication of Pd-MPSS Membrane by Electroless Plating 2

Modeling of Steam Methanol Reforming in Membrane Reactor 16

Steam Methanol Reforming in a Pd-MPSS Membrane Reactor 27

Conclusions 37

Future Work 37

Acknowledgments 37

References 38

INTRODUCTION

The U.S. energy industry is undergoing a profound transformation driven by changes such as deregulation of power generation, increasingly more stringent environmental standards and regulations, global climate change concerns and other market forces. To meet these challenges, the U.S. Department of Energy (DOE) coined a very ambitious (and achievable) plan, what is known as Vision 21 for 21st century. Vision 21 is a pathway to clean, affordable energy achieved through a combination of technology evolution and innovation aimed at developing the most flexible, clean and efficient plants for the 21st century. Recently, U.S. DOE released two documents; "National Hydrogen Energy Road Map," and "A National Vision of America's Transition to a Hydrogen Economy – To 2030 and Beyond," that highlight the emergence of hydrogen as a singular energy source for the future and provide a guideline toward a more secure and cleaner energy future for America [1, 2].

Since the early 1990s, there has been a strong push to develop fuel cells for use in light-duty and heavy-duty vehicle propulsion. A drive for this development is the need for clean, efficient transportation vehicles that can operate on conventional fuels (gasoline, diesel), as well as renewable and alternate fuels (hydrogen, methanol, ethanol, natural gas and other hydrocarbons). With hydrogen as the on-board fuel, such vehicles would be zero emission vehicles. For fuels other than hydrogen, the fuel cell system would use an appropriate fuel processor to convert the fuel to hydrogen, yielding vehicle power trains with very low emissions and high efficiencies. In the Vision 21 roadmap, fuel cell power may provide a viable alternative for the transportation industry to deploy high efficiency, ultra-low emissions vehicles.

In recent years, there has been growing interest in Proton Exchange Membrane Fuel Cell (PEMFC) technologies for down-to-earth applications because of its high power density, high efficiency and almost zero emission to the environment. The major focus on PEMFC technology is to develop fuel cell system for transportatiion applications, which require development of low cost cell components and reliable, high-purity H_2-fuel source. The PEMFC tecghnology is attractive because of its low operating trremperature and ease of start-up. The U.S. Military has a pressing need for lightweight, compact power supplies to support troops in the field and fuel cell-based power system is being evaluated as a major contender to fill the vacuum.

Reformed methanol, liquid and gaseous light hydrocarbons are expected to major fuel source in PEMFCs for terrestrial transportation application. The poisoning of the expensive electrocatalysts by CO in the reformed fuel is a major concern. Crossover of methanol in direct methanol PEMFC is also problematic. Catalytic cracking of ammonia to hydrogen is a serious contender for fuel source. Whether it is reforming methanol, methane and liquid hydrocarbons as a source for hydrogen or cracking of ammonia for hydrogen for fuel cells, separtion of hydrogen at elevated temperature is a major technical issue. In this context, membrane-based technology as fuel process appears very attractive.

The development of palladium-based membranes for high temperature applications has received considerable attention in recent years because of its potential impact in H_2-separtions. Technologically, this could play a significant role in fueling the hydrogen economy. Palladium-based metal membranes are expected to play an important role in selective separation and rapid purification of hydrogen providing high flux at elevated temperatures [3-9]. To provide hydrogen flux in Pd-based membranes that could be commercially viable, the Pd-film has to be in the range of 10 to 15 μm or even less on porous supports such as glass, alumina, nickel and stainless

steel. A number of techniques are available to deposit palladium and its alloy film on microporous support [7, 9]. Most of the applied methods except electroless plating are very limited as membranes prepared by those methods are of low surface area and hence require high operating/fixed costs.

We propose to develop an inorganic metal-metal composite membrane to study reforming of liquid hydrocarbons and methanol by equilibrium shift in membrane-reactor configuration, viewed as fuel processor. Based on our current understanding and experience in the Pd-ceramic composite membrane, we propose to further develop this membrane to Pd and Ad-Ag alloy membrane on microporous stainless steel support to provide structural reliability from distortion due to thermal cycling and hydrogen embrittlement. Because of the metal-metal composite structure, we believe that the associated end-seal problem in the Pd-ceramic composite membrane in planar and tubular configurations would not be an issue.

Our proposed research if successful will have several technological advatages over other conventional hydrogen purification methods which include: (a) Reforming reaction is not limited by thermodynamic equilibrium, as soon as hydrogen is formed, hydrogen is tranported selectively across the membrane, (b) Reforming and separation is carrried out in a single unit, thereby eliminating the need of hydrogen separation and recovery units, and (c) The membrane-reactor-separator (fuel processor) is modular and compact in size and will lead to significant cost and energy savings.

RESEARCH OBJECTIVES

The purpose of this project is to develop hydrogen-selective Pd-Ag composite membrane in microporous substrate for use in production and separation of hydrogen at elevated temperature. The objectives of this research are to:

1. Fabricate H_2-selective Pd-Ag composite membrane in planar and tubular configurations on microporous porous stainless steel substrate by electroless deposition process.
2. Study the H_2-permeation characteristics of Pd-Ag composite membranes using pure hydrogen and mixed gases. Evaluate the membranes for long term integrity and stability under thermal cycling for Pd-Ag film adhesion and H_2-permeation properties.
3. Using tubular Pd-Ag composite membrane, design and fabricate shell-and-tube structured membrane reactor and conduct steam reforming of methanol experiments to study the equilibrium shifts and permeation characteristics.
4. Validate the performance of the membrane-reactor using our previously developed membrane-reactor model for steam reforming of methanol.

FABRICATION OF Pd-MPSS MEMBRANE BY ELECTROLESS PLATING

Electroless plating method has been extensively used in fabricating Pd and Pd-alloy composite membranes for high temperature H_2-separation applications [9-17]. This method offers some advantages over other methods which include: (1) it can be applied in both conducting and non-conducting surfaces, (2) it can be applied to substrate of any size and shape, and (3) plating bath set-up is simple and relatively inexpensive. Electroless plating of palladium is a combination of cathodic deposition of metal and anodic oxidation of reductant in an immersion potential. The

long term performance of the Pd-composite membrane fabricated by the electroless plating is greatly affected by the crystallite distribution and microstructural characteristics of the film [12].

In conventional electroless plating (CEP), oxidation-reduction reactions between Pd-complex and hydrazine (reducing agent) results in metallic deposition of Pd° in a solid surface. An efficient electron transfer between the phases is very important in dense film layer deposition. The surface morphology of the substrate controls the size of Pd grains and degree of agglomeration.

Electroless plating is a three step process: (a) pretreatment of the substrate, (b) sensitization and activation of the substrate surface, and (c) autocatalytic reaction for electroless deposition. The reactions involved in the electroless plating are:

Anodic Reaction: $N_2H_4 + 4OH^- \rightarrow N_2 + 4H_2O + 4e^-$

Cathodic Reaction: $2Pd\left[NH_3\right]_4^{2+} + 4e^- \rightarrow 2Pd^\circ + 8NH_3$

Autocatalytic Reaction: $2Pd\left[NH_3\right]_4^{2+} + N_2H_4 + 4OH^- \rightarrow 2Pd^\circ + N_2 + 4H\ O + 8NH_3$

In this work, we also explored Pulsed Laser Deposition (PLD) assisted activation as alternate method to conventional sensitization and activation process. To understand the plating bath stability, we also studied the Pd+2/EDTA co-ordination kinetics of the electroless plating bath conditions.

Materials and Methods

Pd-MPSS Membrane Fabrication by Electroless Plating

To fabricate robust, reproducible Pd film on microporous stainless steel (MPSS) substrate by electroless plating method, a stable electroless plating bath is an absolute necessity. The quality of the palladium film deposited strongly depends on the bath temperature, rate of deposition and the process of heat treatment [13, 18-20]**.** In this work, we designed robust electroless plating bath for operation under a fume hood. The set-up of the new electroless plating bath is shown in Figure 1.The major design feature of the electroless plating bath are:

- Temperature of the plating bath can be controlled up to 90 °C with an accuracy of ± 0.24 °C.
- Continuous monitoring of bath solution temperature and pH. An ACUMET AP 061 pH digital meter which has an electrode equipped with K-type thermocouple was used for pH monitoring.
- Individual deposition rate of palladium/silver was estimated by taking difference of dry and deposited samples using Mettler Toledo AT 201 micro-balance which can measure within the range up to 0.01 mg (10 μg).
- MasterFlex osmotic solution drive with flow control 500 ml/min to 4 liter/min.

The electroless plating bath can be conveniently used for plating either the inside or outside of the tubular microporous substrate. It can be also used for deposition on planar substrate. As electroless plating is strongly sensitive to in-situ cleaning procedure of substrate, ultrasonic cleaning bath for tube cleaning was installed under the same fume hood. The new electroless plating bath provides improved safety and stability.

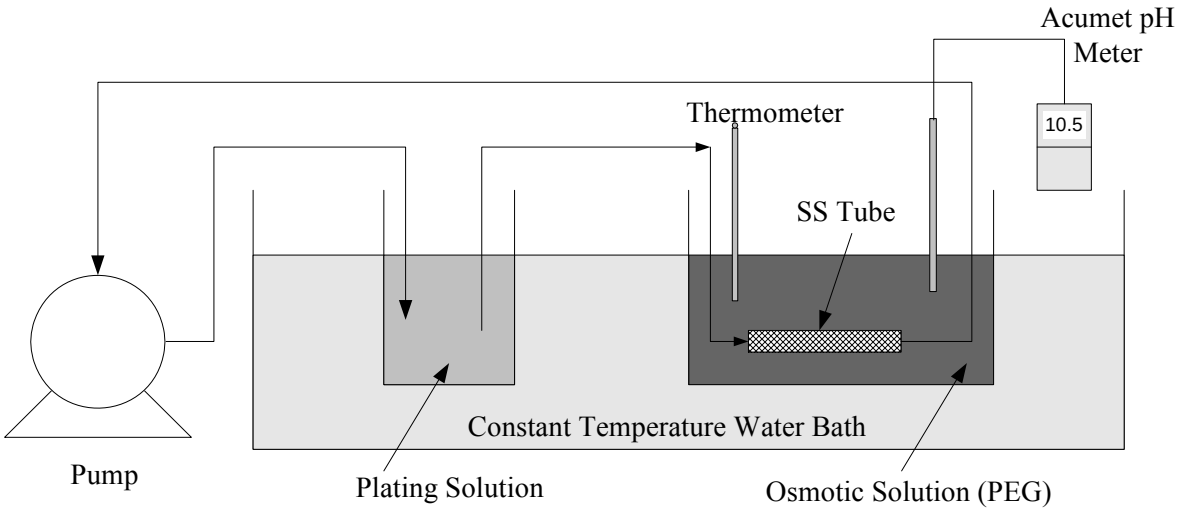

Figure 1. Electroless Plating Bath Setup

All MPSS substrate discs ($1/8^{th}$ inch thickness and 1 inch diameter with nominal pore size of 0.2 μm) and tube (11.2 cm long, 10.07 cm ID and 10.072 OD with nominal pore size of 0.2 μm) used in this study were obtained from Mott Metallurgical Corporation (Farmington, CT, USA). Manufacturer's product information is used to determine average pore size of the substrate. Before sensitization and activation, the MPSS substrates were thoroughly cleaned and dried using carbon tetrachloride and ethanol (Fisher Scientific, ACS reagent grade). The sensitization and activation solutions were prepared using reagent grade $SnCl_2 \cdot 2H_2O$ (Sigma Aldrich, 98%) and $PdCl_2$ (Sigma Aldrich, 99.9%) in hydrochloric acid. For electroless plating, analytical grade ammonium hydroxide and hydrazine (1.0 M) were obtained from Arcos Organic. EDTA sodium salt and tetra-amine palladium nitrate were supplied by Sigma Aldrich.

PLD Assisted Activation of MPSS Substrate

Fabrication of pure and robust palladium film by electroless plating is greatly limited by initial success on activation step of porous rough surface. Surface treatment in activation step is found tedious and in conventional immersion seeding process reproducibility of the activated surface still remains a problem due to variation in the porous surface microstructure from sample to sample. In conventional activation process, undesirable contaminants such as palladium hydroxide ($Pd(OH)_2$), hydrated Palladium ($Pd{\cdot}xH_2O$), palladium chloride ($PdCl_2$), or acetate ($Pd(CH_3COO)_2$), and poorly soluble hydrated stannous chloride ($Sn(OH)_{1.5}Cl_{0.5}$) may be co-deposited in the seeding step [21-24]. To overcome these difficulties, Pulsed Laser Deposition (PLD) as a new surface treatment technique was investigated in our lab. PLD process is widely used in micro-electronic research to fabricate nanometer range superconductive films. In our Lab, we used this technique to activate porous stainless steel substrate. Nano-particle deposited in the rough surface using PLD (as an activation step) was found to improve the Pd-film deposition by electroless plating process and the film was found to be superior in terms of adhesivity and thermal stability.

PLD is extremely simple, probably the simplest among all thin-film growth techniques. As illustrated in Figure 2, it consists of a target holder and a substrate holder housed in a vacuum

chamber. A high-power laser is used as an external energy source to vaporize Pd-target and then the vaporized metal is deposited on the substrate as thin film.

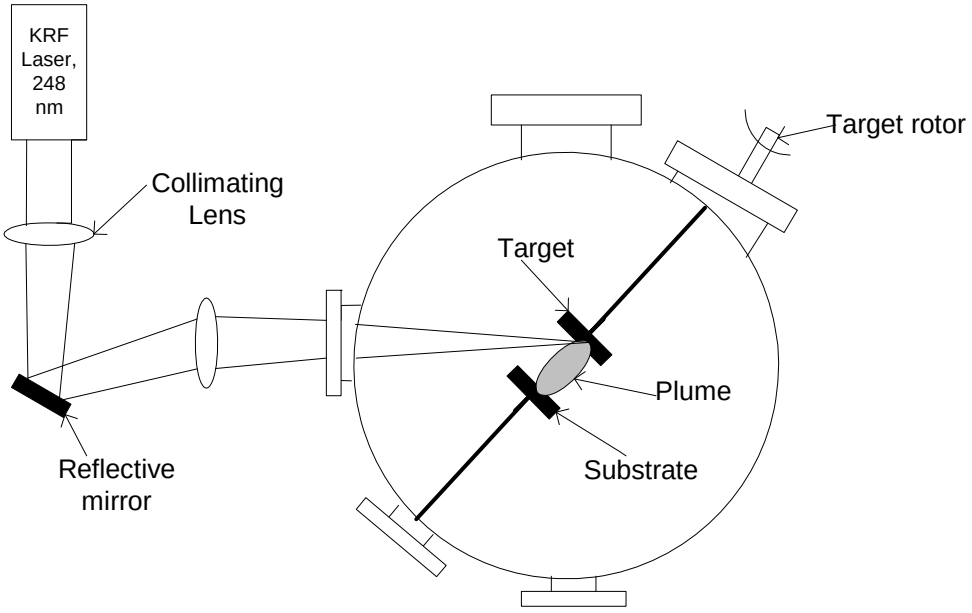

Figure 2. Schematic of Pulse Laser Deposition Process

In order to activate substrate by palladium nuclei, PLD process was carried out using KrF excimer laser (λ = 248 nm, pulse width = 20000 Å, repetition rate = 20 Hz). Before deposition, the PLD chamber was evacuated to a pressure of 10^{-7} mbar. The target used was a 1 inch dia palladium foil of 0.125 in thickness with 99.95% Pd-purity (Kurt J-Lesker Co). Target was mounted in parallel with substrate and laser fluence was maintained 5 J/cm^2. Deposition was carried out on 0.2 μm porous stainless steel disk which was asymmetrically centered in the vacuum chamber.

The surface and pores of the PLD activated MPSS substrate showed considerable deposition of pure palladium nuclei throughout the porous substrate. In the PLD process, generated pulse imparts considerably higher kinetic energy to ablated materials and because of those high energy evaporants and fast response time, produced film possess very strong crystallinity and adhesivity [25]. Therefore, PLD activated layer worked as an intermediate strong adhesive layer between stainless steel support and further deposited palladium membrane. Activation by PLD was completely reproducible and avoided clumsy and repetitive Sn/Pd activation technique. Pd-nuclei formed by PLD process was completely pure, free from any gaseous or metallic contaminants either trapped or compounded since, deposition at the chamber occur at ultra high vacuum environment.

Results and Discussion

Activation and Sensitization

The quality of defect free palladium film strongly depends on activation and sensitization step. The purpose of activation step was to uniformly seed the porous stainless steel substrate (PSS) with palladium (Pd) nuclei. In the past we had difficulty in the reproducibility of the sensitized and activated surfaces. It was observed that complete activation leads to a very smooth and adhesive film [18]**.** In this work, activation step is slightly modified by successive displacement plating of tin (Sn) and palladium (*Pd*) nuclei. In the first step dirt-free ultra-clean substrate is immersed on boiling acidic stannous chloride solution ($SnCl_2$). In the process, ferrous ion (Fe^{++}) in the porous substrate is gradually replaced by stannous ion (Sn^{++}) at about 80 °C [19**]**. Heating at 80 °C helps expand interstitial air in the pores to release into the atmosphere. Consequently, porous substrate instantaneously filled with stannous ion is replaced by palladium seed.

Displacement Plating of Tin (*Sn*) on Iron (*Fe*):

$$Fe \rightarrow Fe^{++} + 2e \qquad\qquad Sn^{++} + 2e \rightarrow Sn$$

Activation of Palladium (*Pd*):

$$Sn \rightarrow Sn^{++} + 2e \qquad\qquad Pd^{++} + 2e \rightarrow Pd$$

The composition of the sensitization and activation bath and the operating conditions are given in Table 1.

Table 1. Composition and operating conditions for activation/ sensitization

	Sn Solution	*Pd* Solution
$SnCl_2$ (g/l)	1.0	
$PdCl_2$ (g/l)		0.1
HCl (M)	0.1	0.1
Temperature (°C)	80	20
Immersion Time (min)	3 - 4	5 - 6

For stable and reproducible film deposition, the immersion of porous tube on stannous chloride solution should not be continued more than 3 to 4 minutes. Otherwise, outer porous substrate would be more porous and completely micro-structurally irregular as the surface is covered by stannous ion. After displacement plating with tin, the substrate is subsequently immersed in acidic palladium chloride solution ($PdCl_2$) at room temperature. After 2 or 3 times of activation, very smooth and uniform shiny seeding of palladium was observed. After activation, substrate was heated in argon environment at 120 °C for 2 hour. EDX analysis (Figure 3 and Table 2) of activated PSS shows that over 15 % of outer surface was covered by palladium seed.

Table 2. Elemental Composition in Activated Palladium Substrate

Element	Specification Type	Element %	Atomic %
Pd-K	EDX	15.36	8.37
Fe-K	EDX	56.76	58.98
Ni-K	EDX	7.8	7.71
Cr-K	EDX	15.27	17.05
Cl-K	EDX	4.82	7.89
Total		100	100

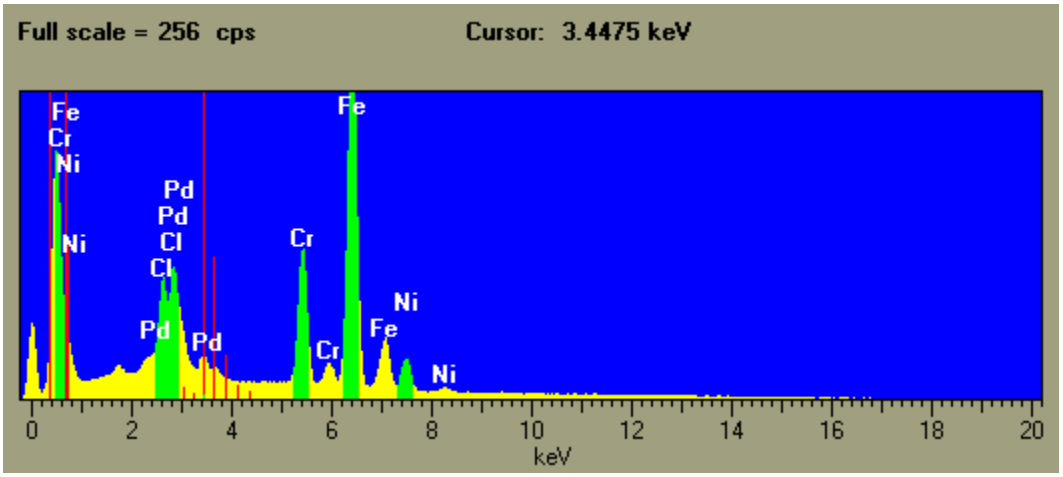

Figure 3. EDX Analysis of Activated PSS Substrate by Displacement Plating

SEM structure (Figure 4) of activated substrate shows a considerable amount of palladium in the outer surface (15.36 %). Activation step would be considered as a sandwich structure of very thin layer with dark-brown color of smooth palladium (*Pd*) screen for subsequent electroless plating. Usually 2 to 3 sensitizing/activation cycles is enough for creating very uniform palladium seeding on the substrate. Otherwise, a thick palladium layer having dense palladium (*Pd*) nuclei on the substrate surface will result that would lower the adhesion of subsequent deposit of *Pd* layers [18].

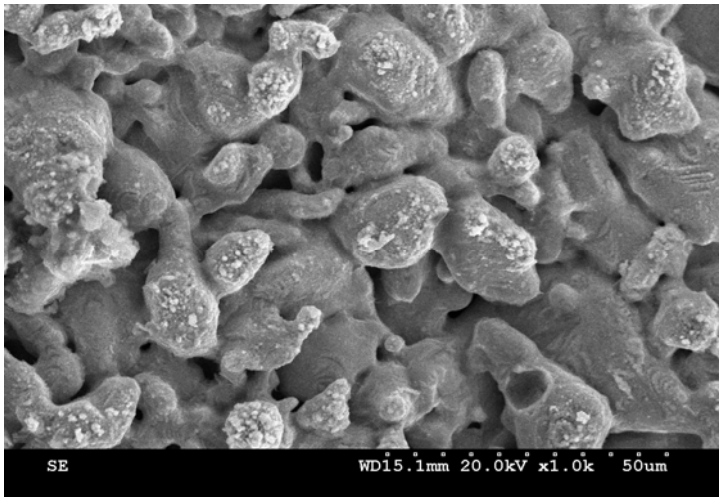

Figure 4. SEM of Activated Layer after 2-cycles of Activation/Sensitization

Modified Electroless Deposition Process

Electroless deposition of palladium was carried out at 55 °C using palladium acetate $(CH_3COO)_2 Pb$ complex. By trial and error, we developed the electroless plating bath solution that was stable. The composition of the electroless plating bath is given in Table 3.

Table 3: Electroless Plating Bath Composition

Electroless Plating Bath	Composition
Palladium acetate $(CH_3COO)_2Pd$,98%	2.0 g/l
Ammonium Hydroxide (NH_4OH), 5.0 N	200 ml
Hydrazine (N_2H_4) 1.0 M	7.2 ml
EDTA salt (Na_2EDTA)	41 g/l
Thiourea (NH_2CSNH_2)	0.0006 g/l
Triton X-100	0.020 g/l
Temperature, °C	55 °C
pH	10.2

Hydrazine was used as reducing agent, and it was added into the plating bath in small proportion during the course of deposition to prevent bulk and course precipitation of palladium (*Pd*). Na_2 *EDTA* was used as chelating agent to prevent precipitation of *Pd*-ion as $Pd(OH)_2$ in the highly alkaline bath [20]. Very small amount of thiourea was used to keep bath stable for longer period [13]. Very small amount of Triton X-100 surfactant (non-ionic) was used for smooth precipitation of palladium nuclei on the porous substrate. Osmotic pressure was maintained by

passing the PEG (Poly Ethylene Glycol, MW 17500, water soluble) inside the porous tube. The plating bath solution appeared to be stable and was able to significantly higher deposition rate. We observed that the surfactant induced electroless plating (SIEP) provides better Pd-grain structures compared to CEP method.

The EDX and SEM analysis of the electroless plated substrate are shown in Figures 5 and 6, respectively. The composition of the *Pd*-film as analyzed by EDX is given in Table 4.

Table 4: Elemental Composition of *Pd*-Film Deposited on PSS Substrate

Element	Specification Type	Element %	Atomic %
Fe-K	EDX	0.3	0.58
Pd-L	EDX	99.70	99.42
Total		100	100

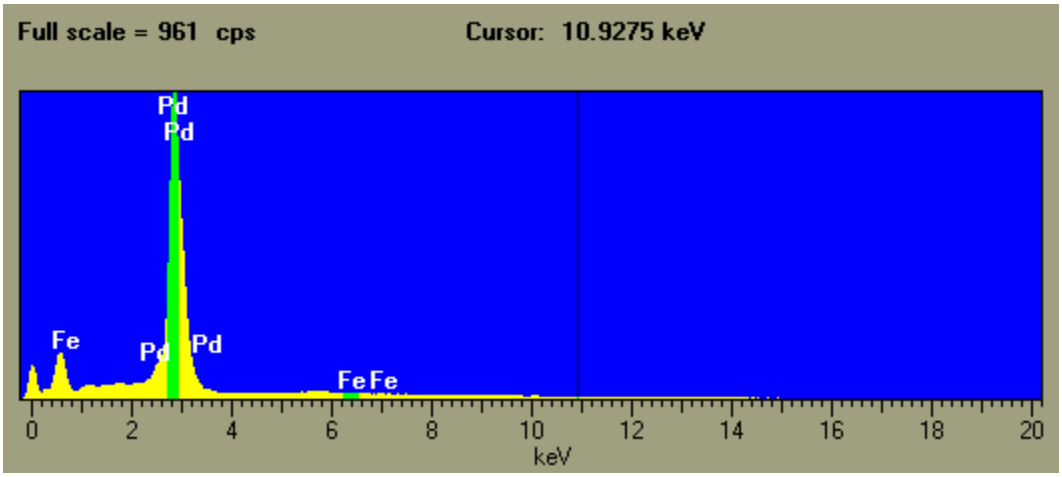

Figure 5. EDX Analysis of Electroless Plated *Pd*-PSS Membrane

The *Pd*-PSS membrane was heat treated in argon environment at 800 °C for about 12 hours. The SEM image indicated that the film was almost smooth without concentrated cellular dislocations. However, thickness of the dense *Pd* layer strongly depends upon largest pores in the support [2]. Membrane permeance would be influenced by orientation, degree of lattice mismatch, rate of nucleation and crystallinity of metal lattice.

Figure 6. SEM of *Pd*-film Annealed at 800 °C in Argon for 12 hours

PLD assisted activation of MPSS substrate

In Figure 7, SEM images of porous stainless still support and PLD activated support with Pd-seeds are shown at 1000 (a – bare support, b – Pd-seeded support) and 5000 (c – bare support, d – Pd-seeded support) magnifications. At 5000 magnifications, Pd-seeds are clearly visible as bright Pd-seeds (nuclei). Penetration of Pd-seeds in the pores is visible. In the conventional Sn/Pd activation process, Pd-seeding in the pores is difficult to achieve.

PLD deposited Pd-seed substrates were analyzed by XRD and EDS. The XRD of the activated Pd- thin-layer by PLD is shown in Figure 8. It shows a distinct palladium peak at 2.2830 Å d-spacing, with lattice (111) orientation. Subsequent electroless plating resulted in deposition of dense, defect free palladium coating, and the membrane appeared to be robust.

In Figure 9, EDS analysis of the sample is shown. An intense peak of palladium as shown in the figure clear demonstrates the quality of the Pd-nuclei as deposited by PLD.

We used the PLD activated Pd-seeds as activated surface and then used this further to deposit Pd-film by using the optimized electroless plating bath. As the Pd-nuclei were seeded uniformly throughout the support surface, autocatalytic electroless deposition of palladium was very uniform and comparatively denser film was produced in relatively thinner coating by subsequent electroless plating. Excellent surface coverage the Pd-film covering most of the surface pores were achieved in electroless plating as during PLD activation steps, larger surface pores (0.2 to 0.5 μm) were seeded with Pd-nuclei. In Figure 10, we show SEM images of a PLD activated electroless Pd-MPSS membrane. The surface microstructure and the x-section view of the Pd-film are shown in Figure 10a and 10b, respectively. The average Pd-film thickness was in the range of 1.43 to 1.79 μm. Thinner film was possible due to excellent seeding by PLD activation. The SEM images were obtained by lighted spot to identify various elemental structures of the Pd-film deposit. Figure 10c shows the x-sectional view of the Pd-film as a continuous structure from surface to surface via pore gap by lighted spot. The elemental composition of the porous support is shown in Figure 10d for iron (Fe-presence), while presence of carbon (C) is shown in

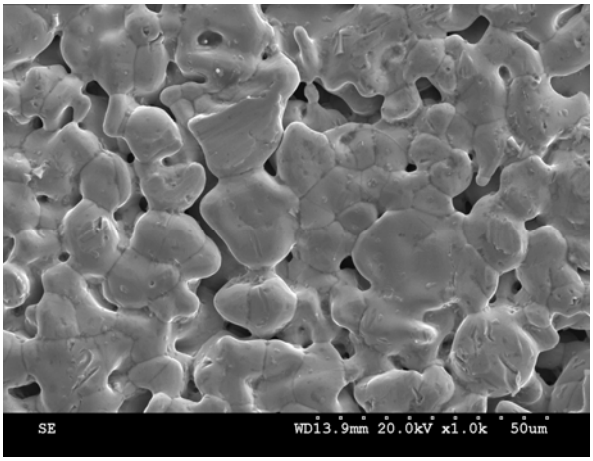

(a) Bare substrate (1k magnification)

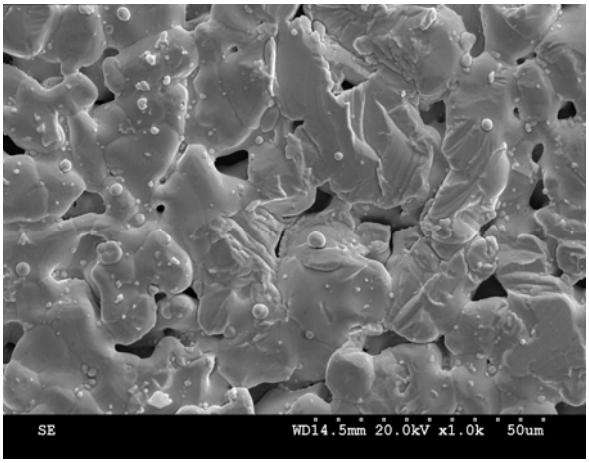

(b) Pd-seeded substrate (1k magnification)

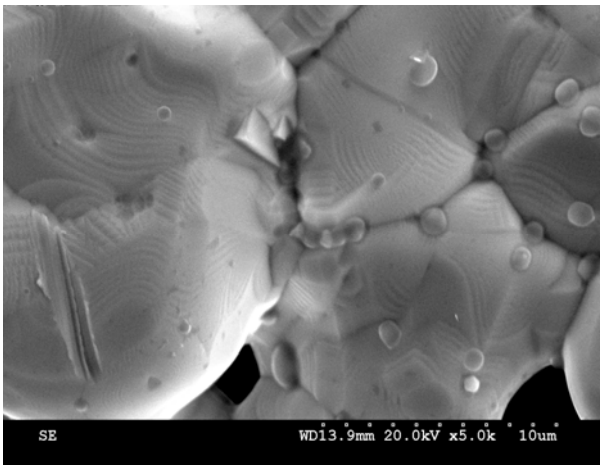

(c) Bare substrate (5k magnification)

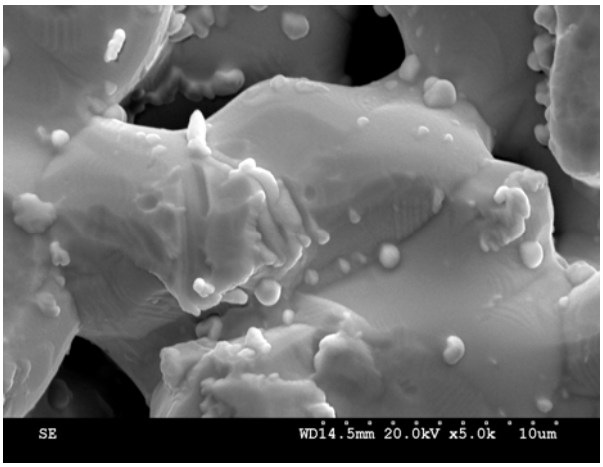

(d) Pd-seeded substrate (5k magnification)

Figure 7. Surface SEM images of bare and PLD activated support surfaces at different magnifications.

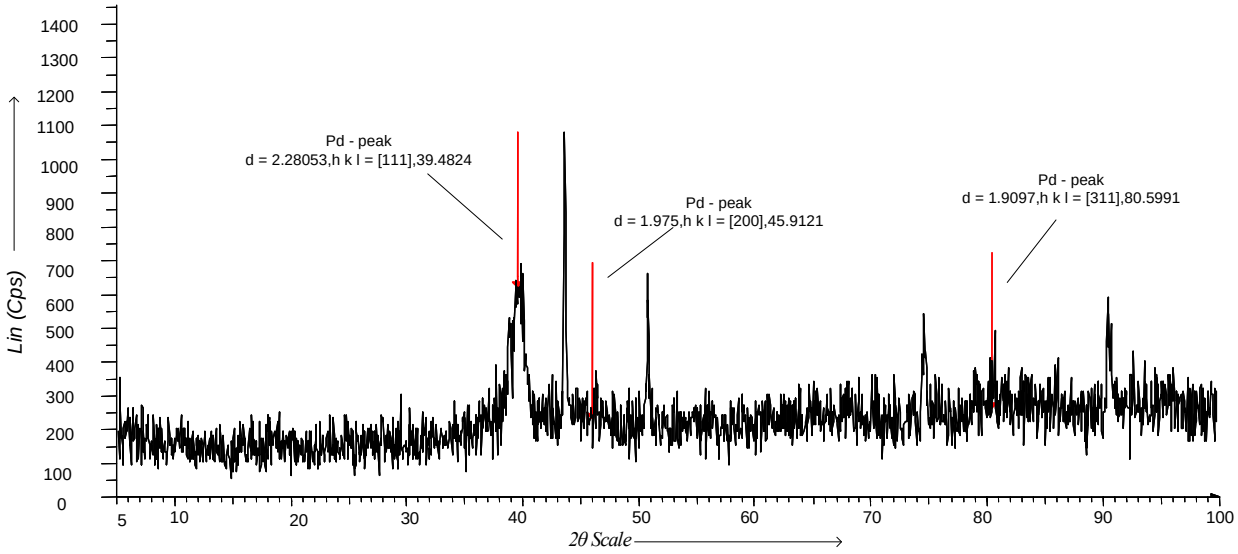

Figure 8. XRD of palladium peak from PLD deposited activation layer (0.5 μm)

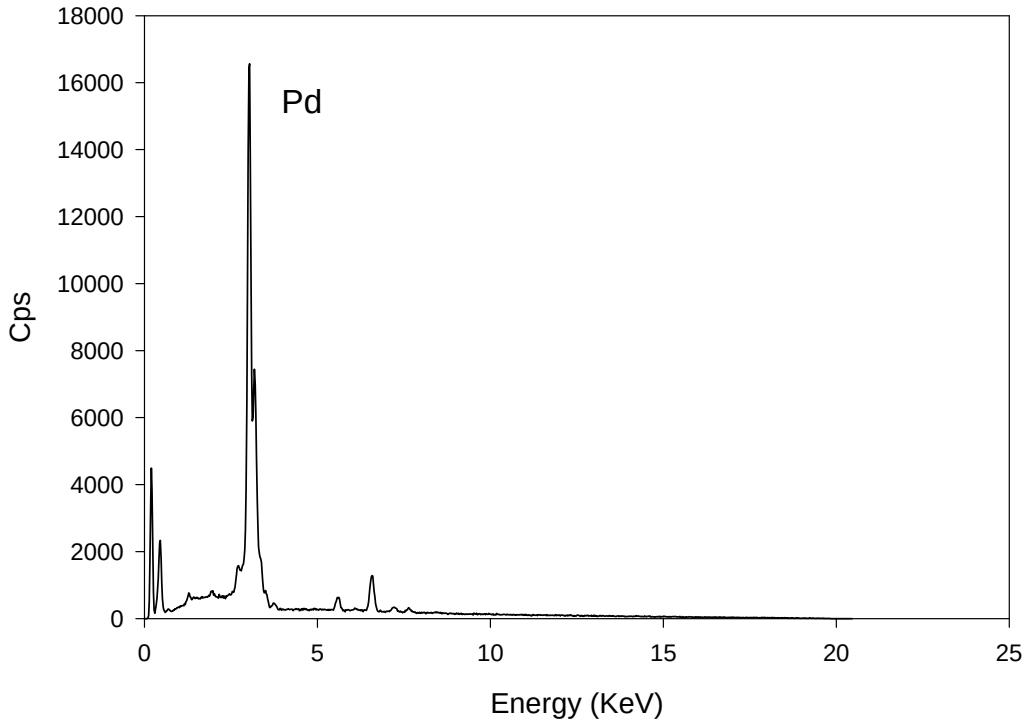

Figure 9. EDS of PLD activated stainless steel substrate

Figure 3.5e in the x-sectional images. The iron oxide layer (diffusion barrier) underneath the Pd-film (blackened layer underneath the lighted Pd-film in Figure 10a) is shown as lighted spot (white shadow) in Figure 10f.

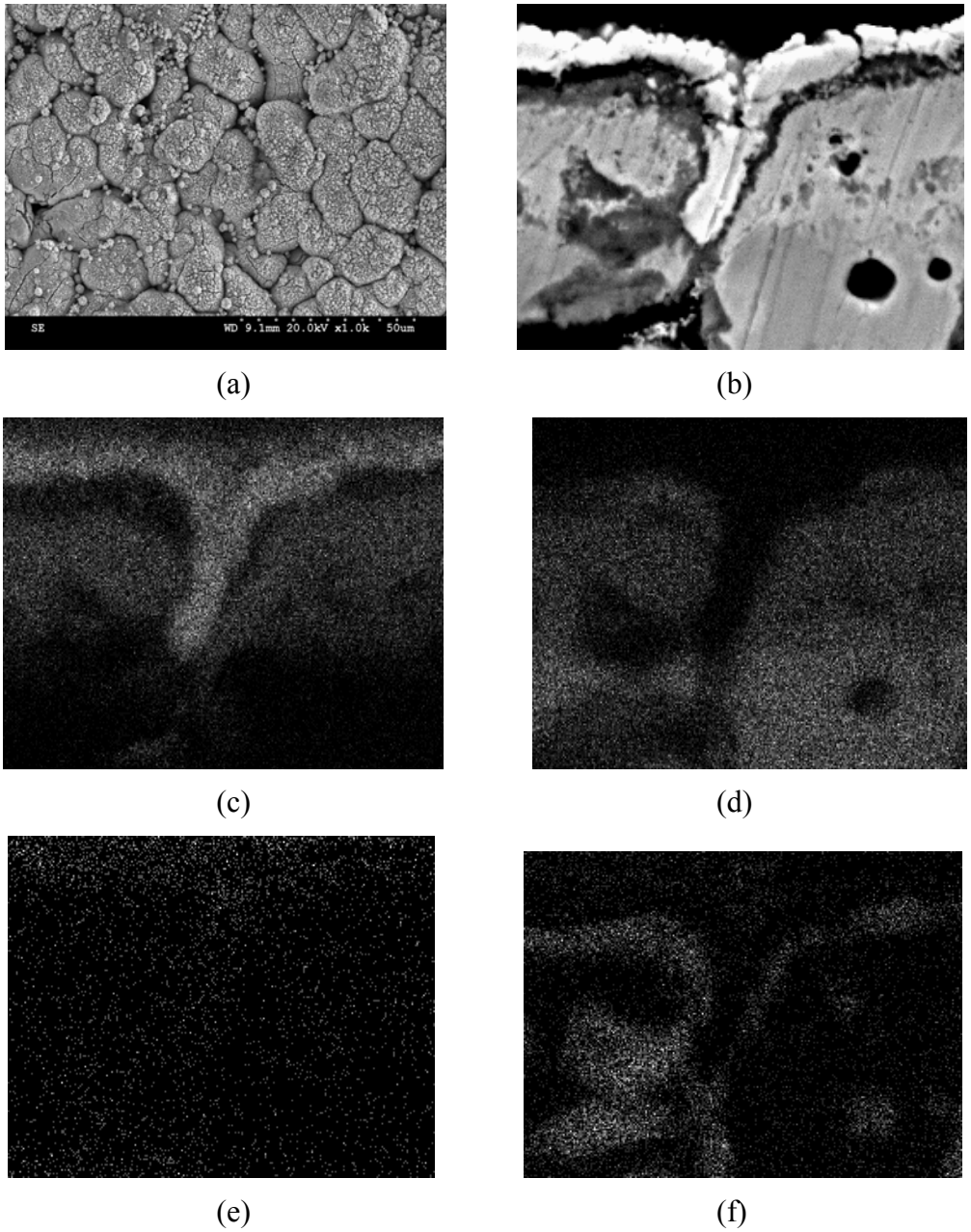

Figure 10. SEM images of deposited palladium film: (a) surface, and (b) cross sectional view; (c) to (f) elemental identification of different layers in cross sections by lighted spot - (c) Pd layer, (d) Fe layer, (e) C- presence, and (f) iron oxide layer.

We tested the Pd-MPSS disc membrane fabricated by PLD activated electroless plating process for hydrogen permeability and selectivity. In Figure 11, hydrogen permeance is shown as a function of transmembrane pressure difference with temperature as a parameter. We carried out permeability measurements in the temperature range of 350°C to 500°C. The hydrogen permeability flux showed a linear relationship with transmembrane pressure difference $\left(\Delta P_{\text{TMP}} = P_H - p_H\right)$ and the hydrogen flux increased with increasing ΔP_{TMP}, For a given ΔP_{TMP}, hydrogen flux increased with temperature.

The transport of hydrogen through dense Pd-film can be expressed in the form of Fick's first law of diffusion as:

$$N_H = \frac{Q_H}{l}\left(P_H^n - p_H^n\right) \tag{1}$$

where Q_H is the hydrogen permeability (a product of solubility and diffusivity), l is membrane thickness, and P_H and p_H are the partial pressures of hydrogen on the high and low pressure sides, respectively.

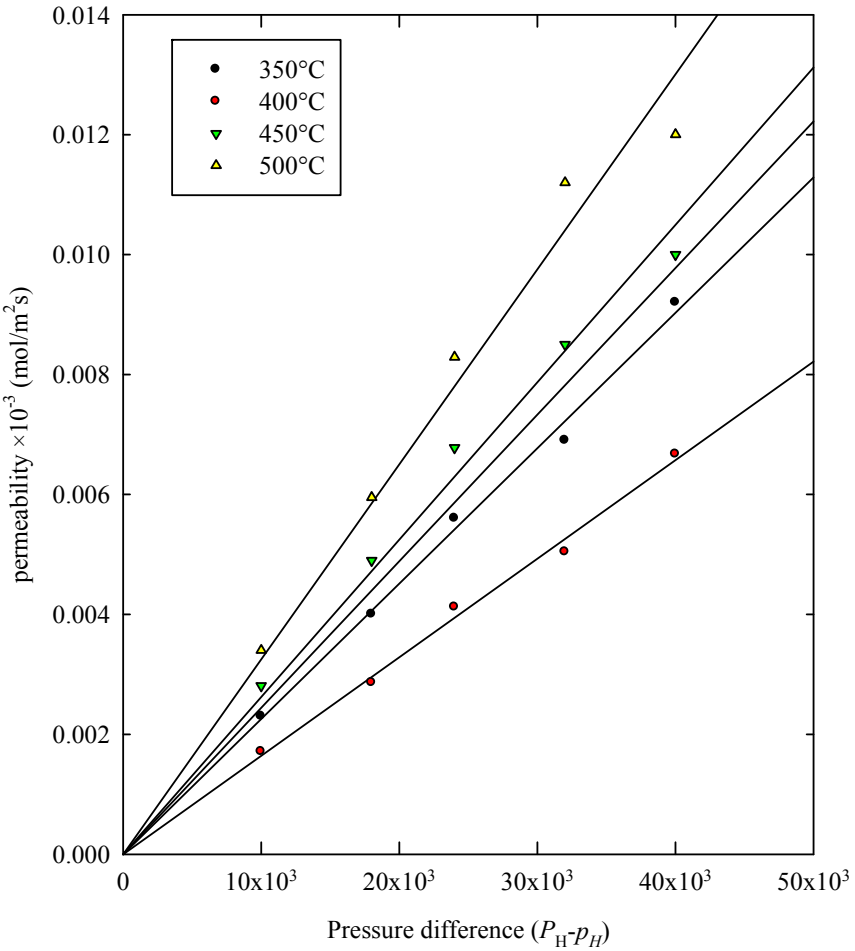

Figure 11. Hydrogen flux of palladium membrane fabricated by PLD assisted electroless plating.

In general, for dense film, the steps involved in H_2-transport are: (1) reversible dissociative chemisorptions of molecular hydrogen on the membrane surface; (2) reversible dissolution of atomic hydrogen in the bulk layers of the metal; and (3) diffusion limiting step and hydrogen atoms form an ideal solution in the metal, n is equal to 0.5, and then Eqn. (1) becomes the Sievert's law and one would expect a linear relationship between the H_2-flux and $\left(P_H^{0.5} - p_H^{0.5}\right)$. Our data shown in Figure 11 deviated from this idealized behavior, and indeed we obtained a power index, $n = 1$, which is valid for transport dominated by surface diffusion. This is applicable to very thin membranes. Our Pd-film was in the range of 1.43 to 1.79 μm, which is extremely thin and the observed results in Figure 11 should not be surprising.

For gas tightness of the Pd-MPSS membrane, we measured the nitrogen flux under conditions similar to that of hydrogen. The nitrogen permeance was fairly independent of temperature and was in the range of 1.35E-10 to 4.25E-09 $\text{mol/m}^2 \cdot \text{s} \cdot \text{Pa}$. The selectivity of hydrogen to nitrogen is shown in Figure 12 over the temperature range of 350°C to 500°C. The selectivity of hydrogen increased with increasing temperature.

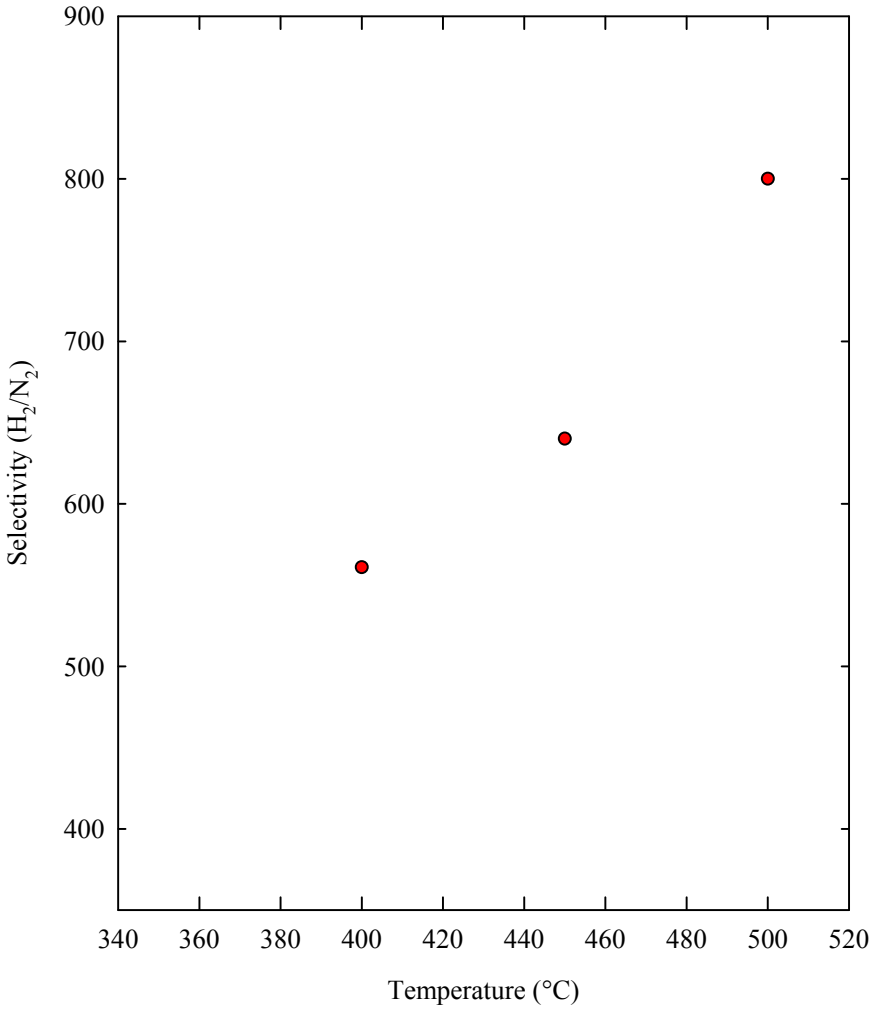

Figure 12. H_2/N_2 selectivity of palladium membrane fabricated by PLD activated electroless plating.

MODELING OF STEAM METHANOL REFORMING IN MEMBRANE REACTOR

Hydrogen is being considered as one of the clean fuel sources for future generations. A major breakthrough would be the utilization of hydrogen in on-board fuel cell technology as a feedstock for most of the vehicular transportation. Steam methanol reforming (SMR) is one of the most important reactions for on-board operations to be considered, since methanol, a major reactant, could be handled as liquid and in high volume. According to the literature, water gas shift reaction and decomposition reaction need to be considered while studying SMR reaction. It is highly desirable to have a kinetic model of SMR, which can predict hydrogen as well as an undesirable carbon monoxide production rate. A significant number of reviews and extensive kinetic studies based on surface reaction mechanisms have been published in the last decade. Notably, Santacesaria and Carra [26] derived Langmuir-Hinshelwood (L-H) form kinetic expression for the reaction rate of methanol reforming. Amphlett et al. [27] investigated the thermodynamic and kinetic aspects of the methanol-steam reforming reaction over $Cu/ZnO/Al_2O_3$ catalysts. Peppley et al., [28] developed a detailed kinetic model for SMR reactions.

Recently, a number of researchers considered hydrogen membrane reactor/separator and simulated the performance methanol steam reforming at different operating conditions [29-33]. Important simulation work by Gallucci and Bassile [32, 33] include the effects of different parameters between co-current and counter-current modes for methanol steam reforming in a membrane reactor. It was found that membrane reactor always offered higher methanol conversion than that of the non-membrane reactor under similar operating conditions. However, in all cases, they oversimplified the simulation results without considering radial concentration gradient, which is obvious during simultaneous reaction and separation in a dense membrane reactor.

In our lab, we are currently developing Pd/Pd-alloy based composite membranes for high temperature applications, with particular interest in hydrogen separation. The Pd-composite membrane was fabricated by depositing thin palladium film on microporous stainless steel tubular support using a novel electroless deposition technique. To evaluate the performance of Pd-based stainless steel microporous membrane in membrane reactor-separator configuration, we investigated the SMR reaction. To better understand the performance of the membrane-reactor, we developed a two-dimensional, pseudo-homogeneous membrane-reactor model for steam-methanol reforming reactions. To account the permeation of hydrogen through the membrane wall in radial direction, radial diffusion was included in the model development. In our earlier modeling work, we only considered reaction in the tube side. In this configuration, the inside of the tube is considered plated with H_2-selective Pd-layer. Currently, we fabricate membranes in tubular configuration by depositing Pd-layer either on the inside of the tube or on the outside of the tube. To account both types tubular membranes, we revisited our modeling work. In this report, we present our modeling work for membrane reactor in shell-and-tube configuration where the reaction takes place in the tube side as reactor (MRT) or shell side as reactor (MRS) and compare the results with the corresponding non-membrane conventional reactors (CRT and CRS).

Model Development

The chemical reactions considered in the SMR are:

$$
\begin{aligned}
&CH_3OH + H_2O \rightleftharpoons CO_2 + 3H_2; \quad && \Delta H_{298\ \mathrm{K}} = 49.51\ \mathrm{KJ \cdot mol^{-1}} \\
&CO + H_2O \rightleftharpoons CO_2 + H_2; && \Delta H_{298\ \mathrm{K}} = -41.19\ \mathrm{KJ \cdot mol^{-1}} \\
&CH_3OH \rightleftharpoons CO + 2H_2; && \Delta H_{298\ \mathrm{K}} = 90.70\ \mathrm{KJ \cdot mol^{-1}}
\end{aligned} \tag{2-4}
$$

Two distinct types of active sites on the catalyst surface are assumed to develop a surface mechanism for the above three reactions. Type 1 site is assumed to be active for methanol steam reforming and water gas shift reaction. Type 2 site is assumed to be active for decomposition reaction. The H_2 adsorbing site associated with the active phase for the methanol-steam reaction and water gas shift reaction is designed as a Type 1a site and the H_2 adsorbing site for the other active phase is designed as a Type 2a site. Based on these catalytic active sites, Peppley et. al [28] developed the following rate expressions:

Methanol-Steam Reaction:

$$
r_R = \frac{k_R K^*_{CH_3O^{(1)}} p_{CH_3OH}}{p^{1/2}_{H_2}} \left[1 - \frac{p^3_{H_2} p_{CO_2}}{k_R p_{CH_3OH} p_{H_2O}} \right] C^T_{S_1} C^T_{S_{1a}} / \left(1 + K^{1/2}_{H^{(1a)}} p^{1/2}_{H_2} \right) \kappa_1 \tag{5}
$$

Water-Gas Shift Reaction:

$$
r_W = \frac{k^*_W K^*_{OH^{(1)}} p_{CO} p_{H_2O}}{p^{1/2}_{H_2}} \left[1 - \frac{p_H p_{CO_2}}{k_W p_{CO} p_{H_2O}} \right] C^{T^2}_{S_1} / \kappa^2_1 \tag{6}
$$

Decomposition Reaction:

$$
r_D = \frac{k_D K^*_{CH_3O^{(2)}} p_{CH_3OH}}{p^{1/2}_{H_2}} \left[1 - \frac{p^2_{H_2} p_{CO}}{k_R p_{CH_3OH} p_{H_2O}} \right] C^{T\ T}_{S_2 S_{2a}} / \left(1 + K^{1/2}_{H^{(2a)}} p^{1/2}_{H_2} \right) \kappa_2 \tag{7}
$$

where,

$$
\begin{aligned}
\kappa_1 &= 1 + K^*_{CH_3O^{(1)}} p_{CH_3OH} / p^{1/2}_{H_2} + K^*_{HCOO^{(1)}} p_{CO_2} p^{1/2}_{H_2} + K^*_{OH^{(1)}} p_{H_2O} / p^{1/2}_{H_2} \\
\kappa_2 &= 1 + K^*_{CH_3O^{(2)}} p_{CH_3OH} / p^{1/2}_{H_2} + K^*_{HCOO^{(2)}} p_{CO_2} p^{1/2}_{H_2} + K^*_{OH^{(2)}} p_{H_2O} / p^{1/2}_{H_2}
\end{aligned} \tag{8-9}
$$

Here k_R, k_W, and k_D are the rate constants for the MSR reactions and corresponding equilibrium constants are denoted by K^*_x, where x represents the subscripted species at the active sites, respectively.

In our modeling work, we used these kinetic parameters and rate equations. The details may be found in elsewhere [34]. A two dimensional heterogeneous model requires a knowledge of effectiveness factors. Methanol-steam reforming (MSR) is a complex reaction and thus defining effectiveness factor for this reaction is difficult. In order to avoid this complexity, a two dimensional pseudo-homogeneous model is assumed to describe the transport mechanism through the catalyst bed. Hydrogen flux through palladium is directly proportional to the product of hydrogen permeability constant and the difference between pressures across the membrane is raised to an exponent n $\left(0.5 < n < 1.0\right)$, which is given as:

$$
N_H = \frac{Q_H}{t} \left(P^n_H - p^n_H \right) \tag{10}
$$

Based on some simplifying assumptions, the continuity equation for any component i may be written as:

$$v_z \frac{\partial C_i}{\partial z} = \left(D_{er}\right)_i \frac{1}{r}\frac{\partial}{\partial r}\left(r\frac{\partial C_i}{\partial r}\right) + R_i + v_Z \qquad (11\text{-}16)$$

where i may stand for argon (1), methanol (2), carbon monoxide (3), carbon dioxide (4), steam (5), and hydrogen (6). For example, $i = 6$ indicates component hydrogen. The production or depletion rates of the components are given by:

$$\begin{aligned} &R_2 = -\left(r_R + r_W\right)S_A; \quad R_3 = \left(r_D - r_W\right)S_A; \qquad R_4 = \left(r_R + r_W\right)S_A \\ &R_5 = -\left(r_R + r_W\right)S_A; \quad R_6 = \left(3r_R + 2r_D + r_W\right)S_A \end{aligned} \qquad (17\text{-}21)$$

The two reactor configurations (MRT and MRS) are schematically shown in Figures 13 and 14, respectively. In absence of membranes, these reactors will be treated as conventional reactor, designated as CRT and CRS reactors, respectively. The reactor dimensions are shown in Figure 15. For the MRT and MRS reactors, the boundary and initial conditions are given as follows:

<u>Tube Side as Reactor (MRT)</u>

BC 1: at $r = 0$ and $0 \le z \le l_o$; $\quad \dfrac{\partial C_i}{\partial r} = 0; \quad i = 1, 2.\cdots, 6$

BC 2: at $r = r_1$ and $0 \le z \le l_o$; $\quad \dfrac{\partial C_i}{\partial r} = 0;$ for $i \ne 6$ and $\left(D_{er}\right)_i \dfrac{\partial C_i}{\partial r} = \dfrac{Q_H}{t}\left(P_i^n - p_i^n\right)$ for $i = 6$

IC 1: at $z = 0$ and $0 \le r \le r_1$: $\quad C_i = C_i^o$ for $i = 1, 2, 5$ and $C_i = 0$ for $i = 3, 4, 6$

IC 2: at $z = 0$ and $r_2 \le r \le r_3$: $\quad C_1 = C_1^o$ and $C_i = 0$ for $i = 2, 3, \cdots, 6$

<u>Shell Side as Reactor (MRS)</u>

BC 1: at $r = r_2$ and $0 \le z \le l_o$; $\quad \dfrac{\partial C_i}{\partial r} = 0; \quad i = 1, 2.\cdots, 6$

BC 2: at $r = r_3$ and $0 \le z \le l_o$; $\quad \dfrac{\partial C_i}{\partial r} = 0;$ for $i \ne 6$ and $\left(D_{er}\right)_i \dfrac{\partial C_i}{\partial r} = \dfrac{Q_H}{t}\left(P_i^n - p_i^n\right)$ for $i = 6$

IC 1: at $z = 0$ and $r_2 \le r \le r_3$: $\quad C_i = C_i^o$ for $i = 1, 2, 5$ and $C_i = 0$ for $i = 3, 4, 6$

IC 2: at $z = 0$ and $0 \le r \le r_1$: $\quad C_1 = C_1^o$ and $C_i = 0$ for $i = 2, 3, \cdots, 6$

The governing partial differential equations, Eqns, (11-16) subject to above initial and boundary conditions are implicitly coupled. They cannot be solved using any regular analytical approach. Introducing concentration of the species in partial pressures, the governing equations, and the ICs/BCs were normalized for numerical solution using finite difference method as marching problem. An iterative scheme was used get converged and stable solution. The details may be found elsewhere [34].

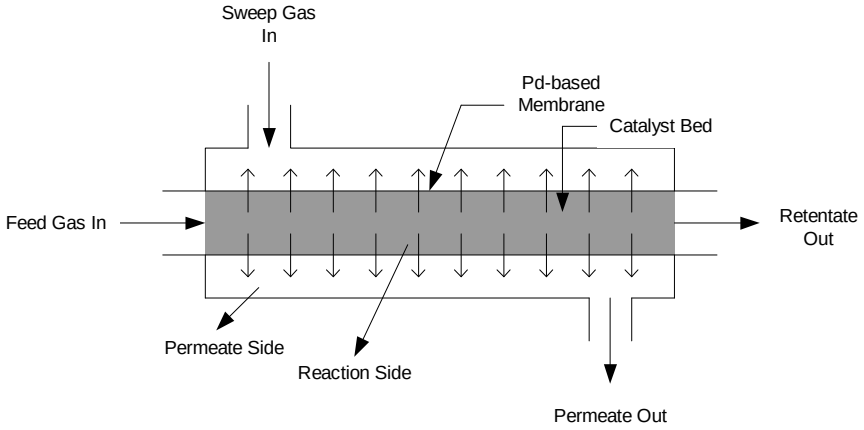

Figure 13. Tube side as reactor (MRT) set-up.

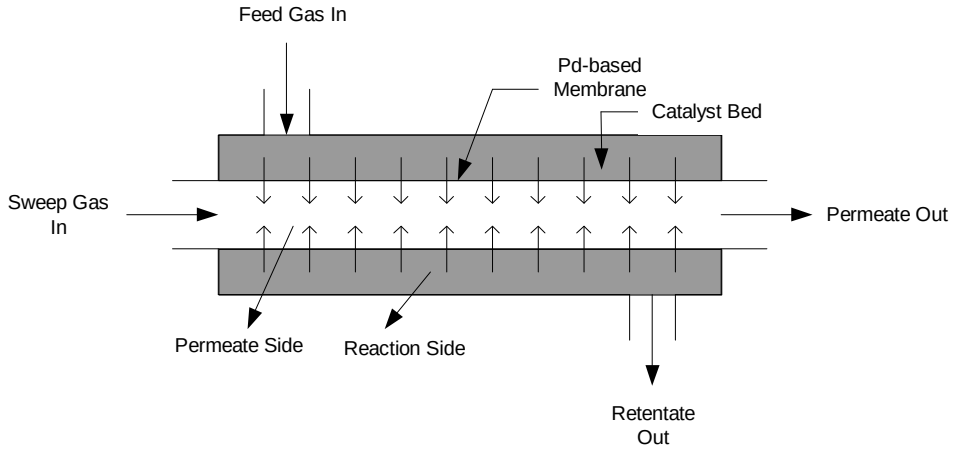

Figure 14. Shell side as reactor (MRS) set-up.

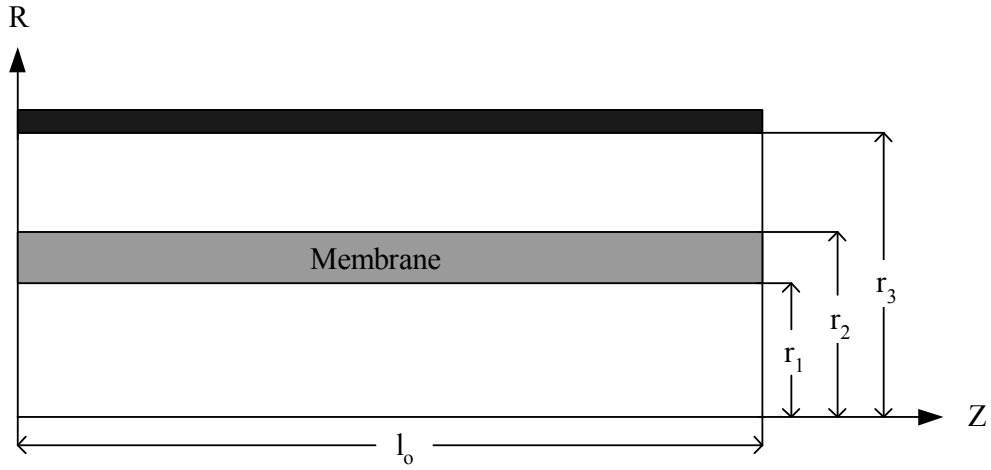

Figure 15. Reactor dimensions.

Results and Discussion

The developed model described above was used to investigate several major operating variables and design conditions using all thermodynamic values for the reaction species and kinetic expression. The rate equations including kinetic and absorption parameters was taken from Peppley et al., [28]. The methanol steam reforming (MSR) reactor parameters used in this simulation study are as follows:

Reactor Dimensions

Total reactor length, l_o = 0.1 m Inner diameter of tube, D_i = 1.070 cm

Outer diameter of tube, D_{ot} = 1.072 cm Inner diameter of shell, D_{os} = 1.512 cm

Catalyst Properties

Commercial catalyst (BASF K3-110) Catalyst diameter: 0.25 mm - 0.35 mm

Catalyst composition: CuO (40%), ZnO (40%), Al_2O_3 (20%)

Pore volume: 0.35 ml/gm BET surface area: 100 m^2/gm_{cat} Catalyst weight: 21.58 gm

Permeation Parameters

Pd/SS membrane thickness, H = 10 μm Power index: n = 0.5

H_2- permeation activation energy, E_p = 15.7 KJ/mol

Pre-exponential factor, $Q_o = 9.596\times10^{-6}$ mol/m.s.$Pa^{0.5}$

Mean pore diameter of SS support: D_p = 0.2 μm

Operating Conditions

Reactor Pressure, P_r = 2 to 10 bar Permeate Side Pressure, P_s = 1.0 bar

Reactor Temperature, T = 200 to 300 °C Time factor (Kg_{cat}.s/mol_{CH3OH}) = 1 to 10

Steam to Methanol ratio, S/M = 2 to 10 Sweep gas (Ar) flow = 2.2×10^{-3} mol/s

Shell side and tube side were separately treated as different reaction zones in order to understand the effects of various reaction parameters. Figures 16 and 17 show the effect of reaction pressure on both the shell side (MRS, CRS) and tube side (MRT, CRT) reaction configurations. In the case of non-membrane reactors (CRS and CRT), there is a positive effect on methanol conversion in a very low range of pressure. However, in a wide range of high pressure region, there must be a negative feedback on all over zones of reaction. In case of membrane counter parts, whatever the ranges of pressure, methanol conversion always increases with the increase of pressure. There are two opposite effects that need to be considered to explain the fact: a) an increase in the reactor pressure negatively affects the methanol conversion according to Le Chatelier's principle, and b) higher reactor pressure provides higher driving force for hydrogen permeation which leads to higher methanol conversion (Figure 18). Thus, whenever reaction products are formed as reaction proceeds, a portion of product is instantly removed from the reactor. Removal of the product from the reactor space shifts the reaction at the right side, that is, more products are supposed to be found and hence a higher conversion is achieved. Thus the second effect prevails throughout the reactor pressure investigated.

The effect of time factor in overall conversion is illustrated in Figures 18 and 19. Time factor (TF) is defined as weight of catalyst (kg) per molar flow rate (mol/s). Higher value of time factor means higher surface areas offered to the reactants, if constant molar flow rate is assumed. Hence, with the increase of time factor, methanol conversion was found to be increasing in the case of both membrane and non-membrane reactors at any configurations. However, at any fixed

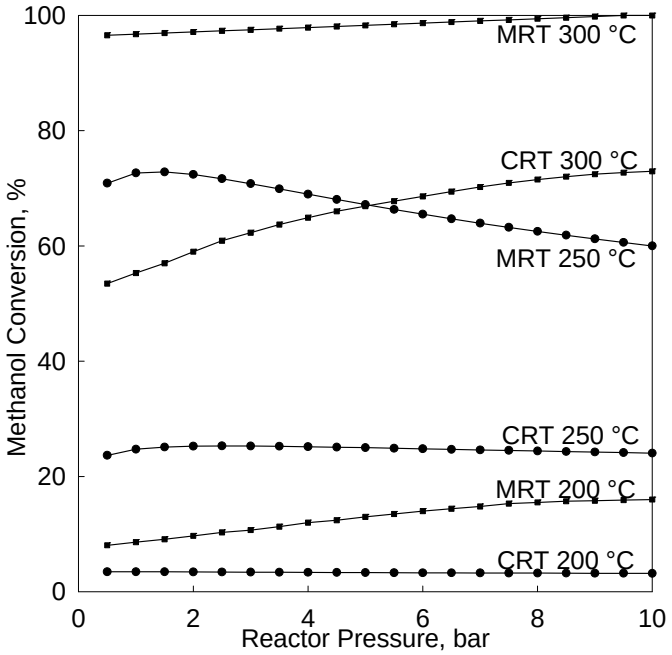

Figure 16. Methanol conversion vs. reactor pressure at various temperatures for MRT and CRT models (P_s = 1 bar, S/M = 1, TF = 10, and sweep gas flow = 2.2×10^{-3} mol/s).

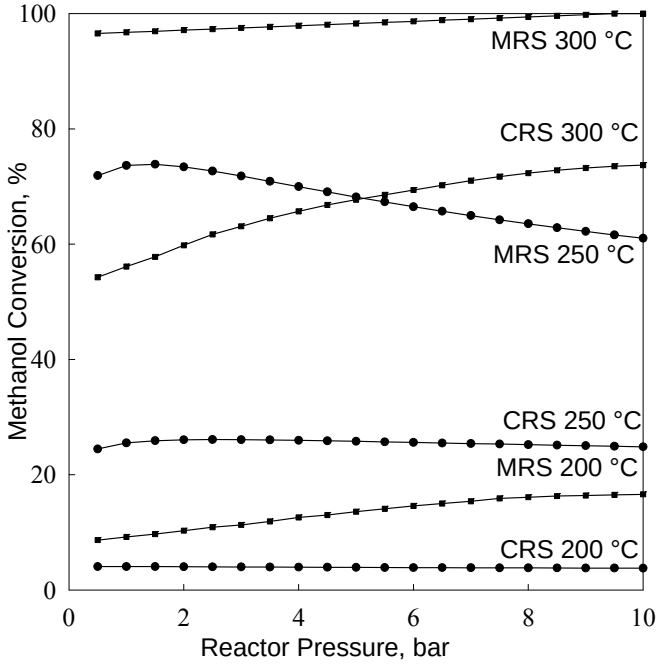

Figure 17. Methanol conversion vs. reactor pressure at various temperatures for MRS and CRS models (P_s= 1 bar, S/M = 1, TF = 10, and sweep gas flow = 2.2×10^{-3} mol/s).

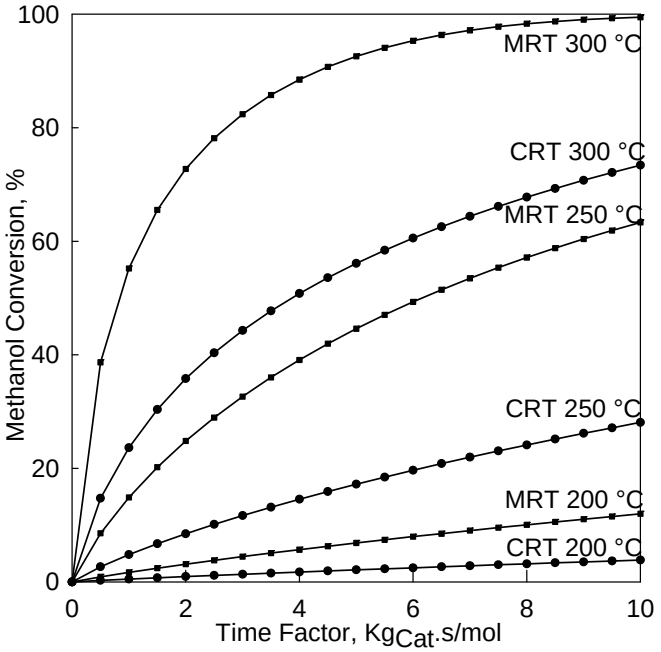

Figure 18. Methanol conversion vs. time factor at various temperatures for MRT and CRT models (P_r = 2 bar, P_s = 1 bar, and sweep gas flow = 2.2×10^{-3} mol/s).

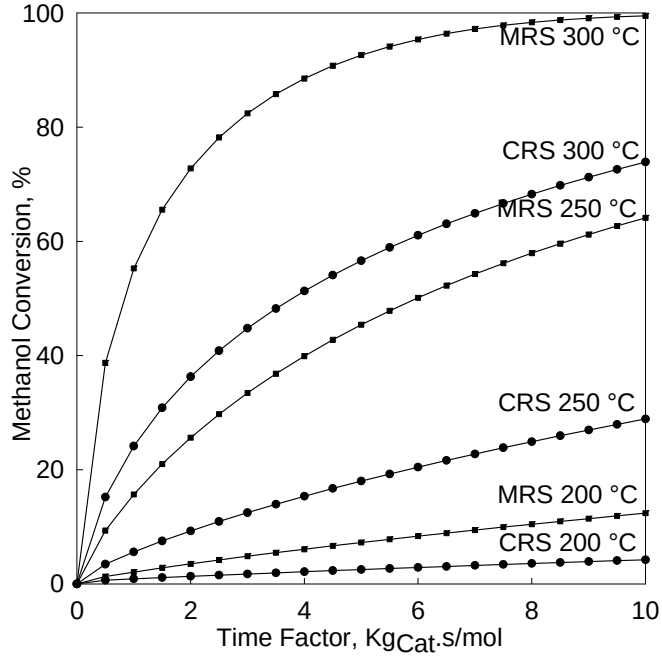

Figure 19. Methanol conversion vs. time factor at various temperatures for MRS and CRS models (P_r = 2 bar, P_s = 1 bar, and sweep gas flow = 2.2×10^{-3} mol/s).

temperature and time factor, conversion in membrane reactor was found to be significantly higher than that of non- membrane counter part due to continuous removal of hydrogen.

The effect of steam/methanol (S/M) ratios on both membrane and non-membrane reactors are illustrated in Figures 20, 21, and 22. Methanol conversion, as shown in Figures 20 and 21, increases with the increase of S/M ratios in non-membrane reactors. In contrast, there is a negative impact on methanol conversion for the membrane counterpart. It can be explained in the following ways: a) for the membrane reactor, increase of S/M reduces percentage of hydrogen recovery, as illustrated in Figure 22, which indirectly reduce methanol conversion, and b) in non-membrane reactor, increase of overall flow rate of methanol impacts positively on conversion.

Overall steam methanol reactions are endothermic in nature. Additionally, permeability of hydrogen can be explained by Arrhenius equation, which means permeability of hydrogen through Pd-membrane increases exponentially with temperature. Because of these two positive effects, methanol conversion is highly sensitive to reaction temperature. As explained in Figures 23 and 24, in low temperature range, there are no appreciable differences in conversion between membrane and non- membrane reactors. However, conversion increases almost exponentially with temperature in membrane reactor of any configurations and it is almost more than double compared to non membrane counterpart.

Simulated results were compared with experimental results for the non-membrane reactor. Methanol conversion at two different temperatures with varying time factors was experimentally determined by Peppley et al., [28]. Experimental results show an excellent agreement with our simulated results considering identical operating conditions as illustrated in Figure 25.

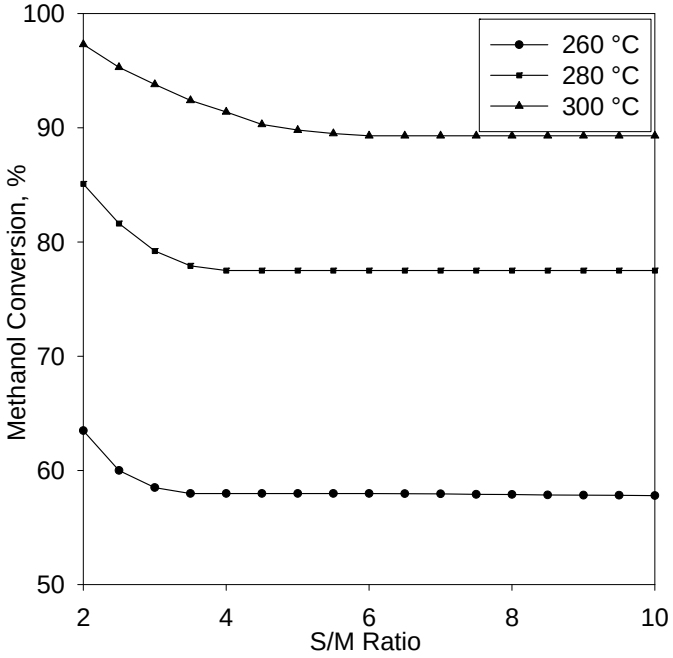

Figure 20. Methanol conversion vs. S/M ratio at various temperatures for MRT model (P_r = 6 bar, TF = 10, P_s = 1 bar, and sweep gas flow = 2.2×10^{-3} mol/s).

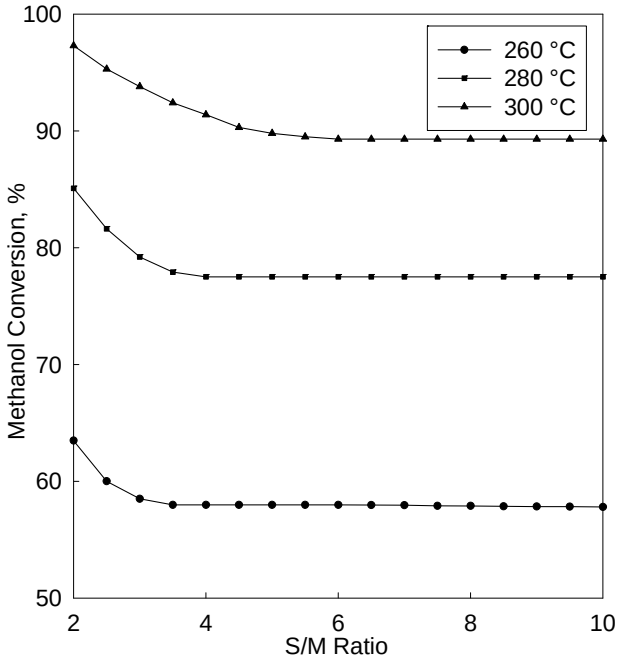

Figure 21. Methanol conversion vs. S/M ratio at various temperatures for MRS model, P_r = 6 bar, TF = 10, P_s = 1 bar, and sweep gas flow = 2.2×10^{-3} mol/s.

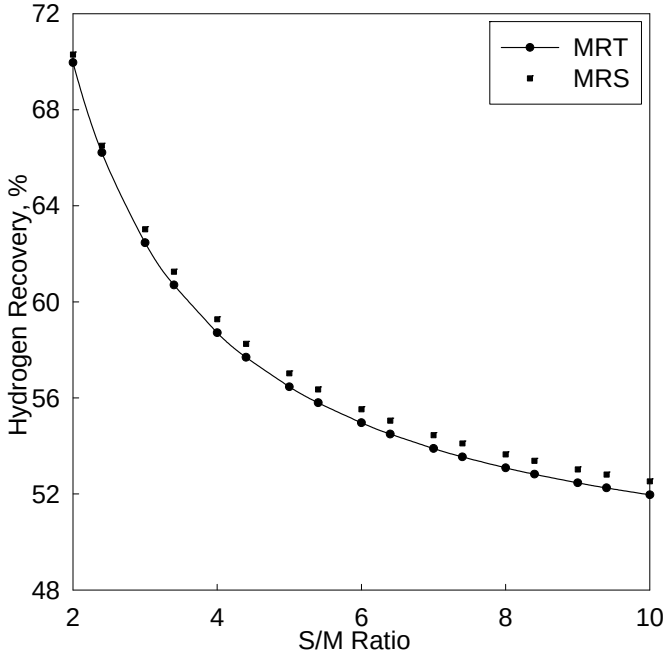

Figure 22. H_2-recovery vs. S/M ratio for MRT and MRS models (P_r = 6 bar, T = 250 °C, P_s = 1 bar, and sweep gas flow = 2.2×10^{-3} mol/s).

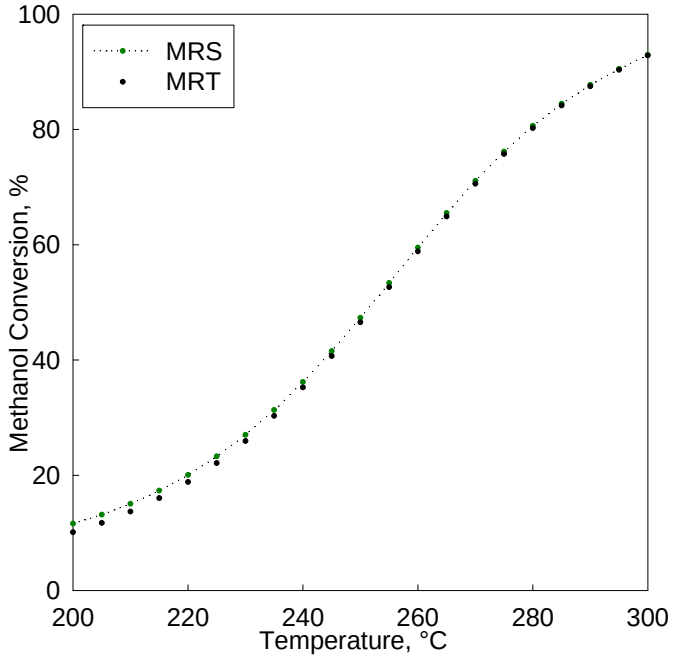

Figure 23. Methanol conversion vs. temperature for MRT and MRS models (P_r = 2 bar, P_s = 1 bar, Sweep gas flow = 2.2×10^{-3} mol/s, and S/M = 3).

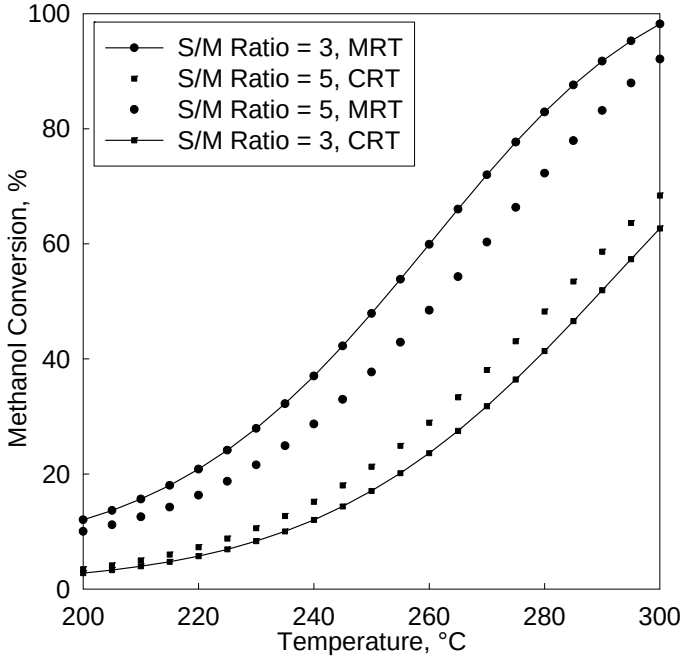

Figure 24. Methanol conversion vs. temperature at different S/M ratios (TF = 10, P_s = 1 bar, P_r = 2 bar, and sweep gas flow = 2.2×10^{-3} mol/s).

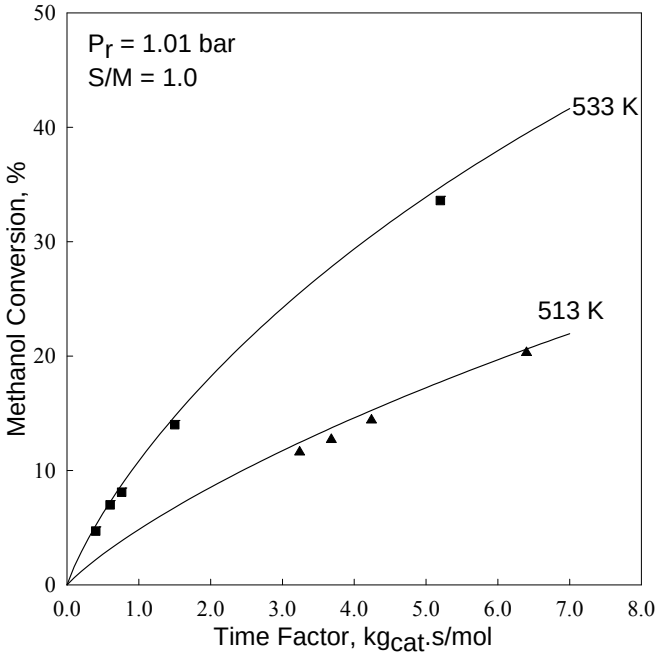

Figure 25. Methanol conversion vs. time factor, simulation and experimental data comparison [26].

STEAM METHANOL REFORMING IN A Pd-MPSS MEMBRANE REACTOR

In the previous section, we presented a 2-D membrane reactor model for steam methanol reforming (SMR). In this part we present our experimental study of SMR in a Pd-MPSS membrane reactor.

The Pd-MPSS membrane used in this study was fabricated by a novel electroless plating process, what we call surfactant induced electroless plating (SIEP). In conventional electroless plating, oxidation-reduction reactions between Pd complex and hydrazine (reducing agent) results a metallic deposition of Pd^0 in a solid surface from the liquid phase solution, an efficient electron transfer between the phases is very imperative in dense film layer deposition. The substrate surface morphology controls the size if Pd grains and degree of agglomeration. The oxidation-reduction reactions between Pd-complex and hydrazine result in evolution of ammonia and nitrogen gas bubbles. When adhered to the substrate surface and in the pores, these gas bubbles hinder uniform Pd-film deposition. To address the problem associated with the growing gas bubbles within the plating substrate vicinity, we explored the role of surface active agents with favorable structures in the electroless plating process [35]. We found that amongst nonionic (Triton X-100 – octyl-phenol ethylene oxide), cationic (DTAB – dodecyl trimethyl ammonium bromide), and anionic (SDBS – dodecyl benzo sulfonic acid solium salt) surfactants, cationic surfactant DTAB was very effective in electroless plating and enables the deposition of a robust thin-film with excellent grain structures.

In our proposal objectives, we planned to develop Pd-Ag composite membrane. We could not move into this work as we spent significant of our effort in perfecting the SIEP method. We are confident that we will be able to extend SIEP to Pd-Ag system in our future work.

Experimental Methods

Pd-MPSS membrane was fabricated on tubular support in our lab by a novel electroless plating method. Microporous stainless steel tubular support elements were obtained from Motts Corporation. The Pd-MPSS membrane in shell-and-tube configuration was used as membrane reactor. Pd-film was deposited by SIEP on the outside of the MPSS tube. SMR reaction was carried out in the shell-side of the shell-and-tube membrane reactor. The dimensions and other characteristic properties of the Pd-MPSS membrane-reactor are given in Table 5.

Table 5. Operating conditions used in SMR during experimental investigations

Operating Parameters	Range
Temperature (°C)	200 to 300 (±10)
Pressure (psi)	14.7 to 50
Methanol flow rate (mol/s)	1.598×10^{-04} to 8.6×10^{-04}
Sweep gas (argon) flow rate (mol/s)	2.2×10^{-03} (constant)
Steam to methanol ratio (mol ratio)	1 to 4
SMR Catalysts	
CuO	24%
Al_2O_3	76%
Catalyst surface area (BET)	100 cm^2/gm-cat

A photograph of the experimental set-up is given in Figure 26. Aqueous solution methanol with predetermined water/methanol mole ratio was charged to vaporizer by a syringe pump. The vaporized methanol-water vapor mixture was then passed through the preheater before feeding into the shell-side of the membrane reactor. The shell-side of the reactor was loaded with catalyst for SMR.

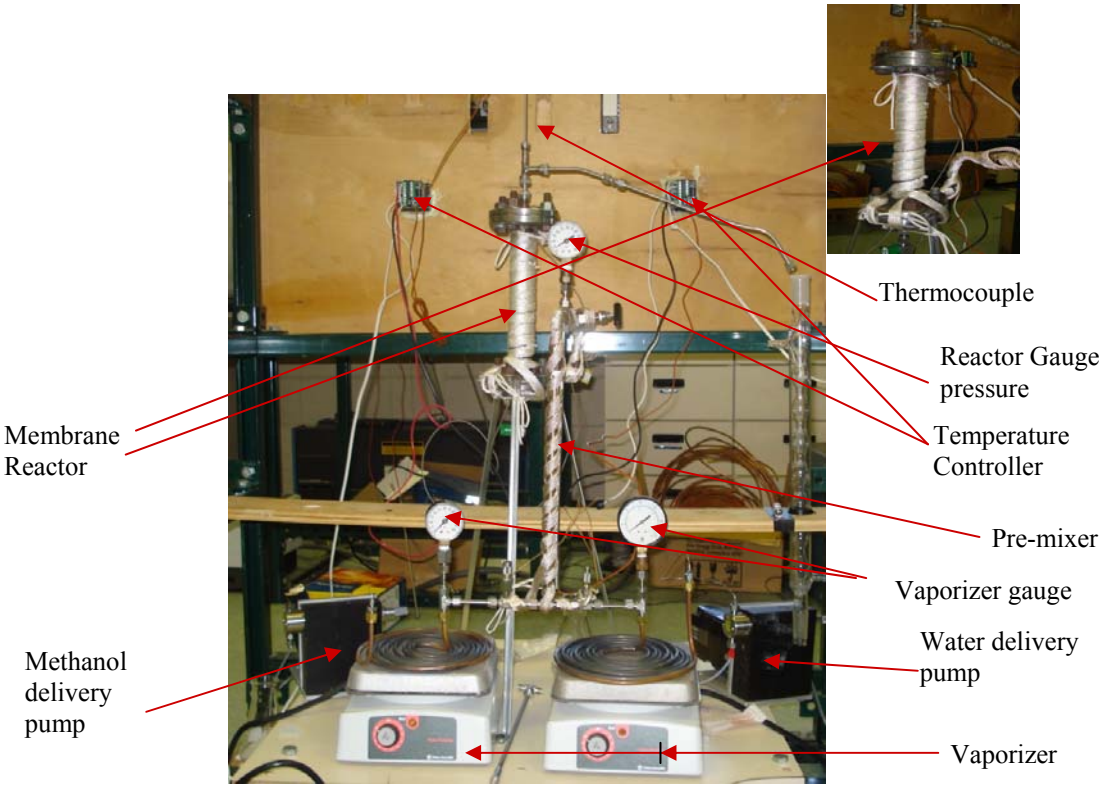

Figure 26. Photograph of membrane reactor set-up for SMR study

Product hydrogen permeates the Pd-MPSS membrane from shell-side (reaction zone) to tube side. All unconverted reactants and products then allowed passing through nitrogen condenser trap where unconverted methanol and water were trapped in liquid nitrogen holder. Both reactor and permeate exit gas streams were analyzed by gas chromatograph. A HP GC (Model No 6890) which was connected to PC for data acquisition and storage was used for gas analysis. The GC was equipped with molecular sieve 5A and carbon plot Q columns. Column isolation techniques were used to analyze CO, H_2, CO_2, Ar and/ or N_2 simultaneously. Unreacted methanol water trapped in the condensate was measured separately in order to calculate methanol conversion during reaction. The operating conditions and process variables used in this study for SMR in Pd-MPSS membrane reactor are given In Table 6. The SMR reaction was carried out using commercial catalyst from supplied from Alfa Aesar Inc.

Table 6. Pd-MPSS membrane reactor dimension and membrane/membrane support properties used in modeling and experimental study of SMR.

Membrane Reactor Parameter	Values
Membrane length	112 mm
Inner tube radius	5.035 mm
Inner tube outer radius	5.036 mm
Shell tube inner radius	6.023 mm
Membrane effective area	7.21E-06 m^2
Membrane permeance constant	1.791×10^{-06} mol/(m-s-$Pa^{0.56}$)
Power index in Sievert's law	0.56
Membrane thickness (Pd-film)	24.3 μm
MPSS tube pore size	0.2 μm
MPSS tube porosity	0.65

Results and Discussion

The H_2-transport characteristics of the tubular Pd-MPSS membrane used in membrane reactor is given in Table 6. We investigated the SMR in Pd-MPSS membrane reactor in the temperature range of 200°C to 300°C for methanol conversion and hydrogen recovery for specified steam to methanol feed ratios and catalyst loadings. The experimental results were compared with SMR membrane reactor model.

The conversion of methanol as a function of catalyst time factor is shown in Figure 27 for three temperatures (200°C, 250°C, and 300°C). The catalyst time factor (space time) is defined as amount of SMR catalyst (in kg) per mole of methanol feed per second. Experimental conversion of methanol is compared with the membrane-reactor model prediction. For a given catalyst time factor, methanol conversion increased with increasing temperature, a trend that is validated by the model prediction. The range of catalyst time factor investigated was in the range of 6.5 kg-s/mol to 9.2 kg-s/mol (Figure 27). At 200°C, the methanol conversions increased from 15% to 18% with corresponding time factors 6.5 kg-s/mol to 9.2 kg-s/mol, respectively. On the other hand, the increases in methanol conversions were 37% to 41% and 62% to 78% at 250°C and 300°C, respective for the same range of catalyst time factor. We observed that at low temperatures, the increased time factor has little effect on methanol conversion. For example, at 200°C and 250°C, the conversions increased by 3% and 5%, respectively for a change in catalyst time factors from 6.5 kg-s/mol to 9.2 kg-s/mol. This marginal increase in conversions may be attributed to low catalytic activity at low temperatures. On the other hand, at 300°C we observed a 16% increase in methanol conversions due to higher catalytic activity.

The effect of temperature on methanol conversion for a methanol flow rate of 8.6×10^{-04} mol/s with catalyst time factor of 9.2 kg-s/mol is illustrated in Figure 28. In this example, the methanol conversion increased from 15% at 200°C to 78% at 300°C. These conversions are higher than equilibrium conversions in fixed-bed conventional reactor [28]. The overall reaction in SMR is

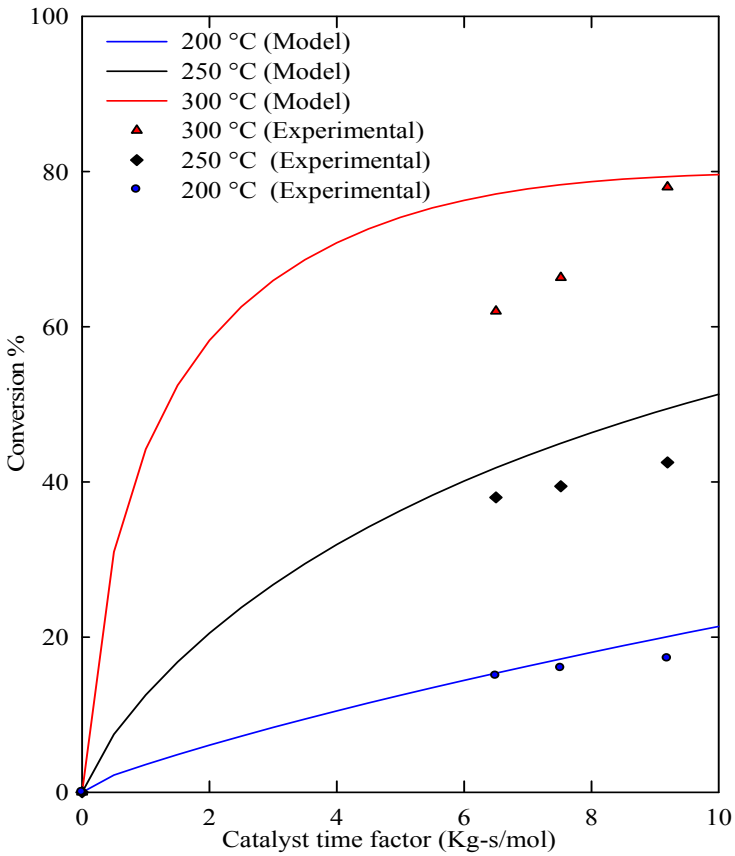

Figure 27. Effect of catalyst time factor on methanol conversion in membrane reactor (operating conditions: methanol flow rate = 8.46 $\times 10^{-04}$ mol/s, steam to methanol ratio (S/M) = 1, reactor side pressure = 50 psi, permeate side pressure =14.7 psi, and catalyst loading = 5.56 gm).

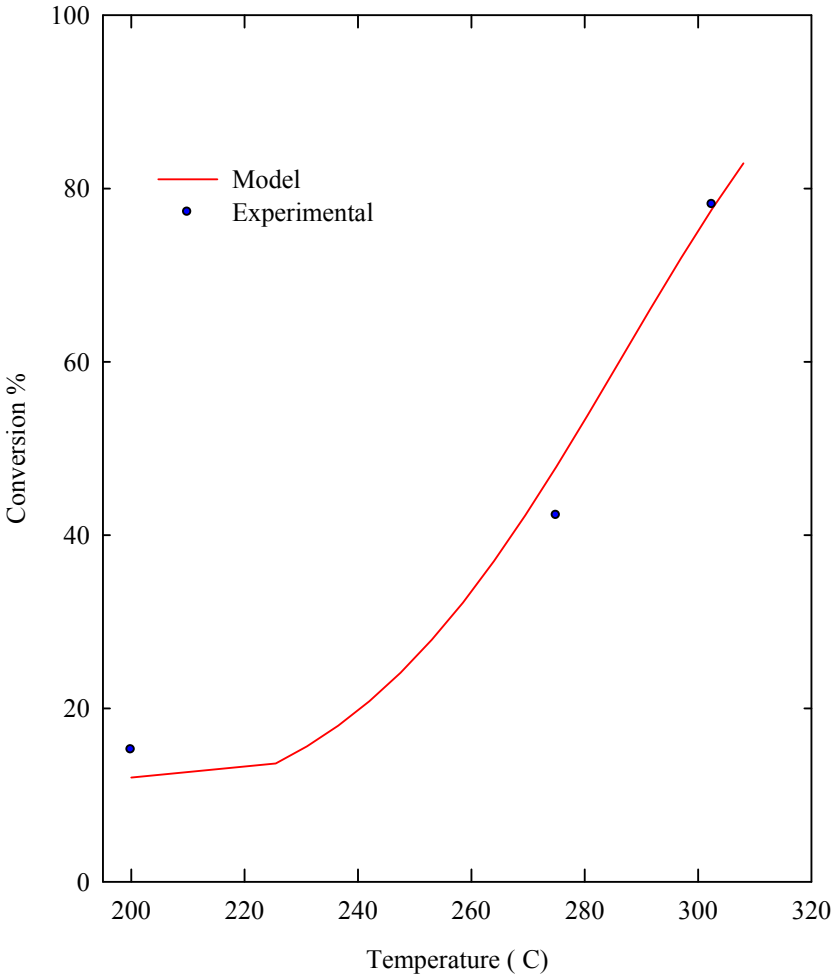

Figure 28. Effect of temperature on methanol conversion in membrane reactor (operating conditions: methanol flow rate = 8.46 $\times 10^{-04}$ mol/s, steam to methanol ratio (S/M) = 1, reactor side pressure = 50 psi, permeate side pressure =14.7 psi, and catalyst loading = 5.56 gm).

endothermic which favors higher reaction rate with increased temperature. In the membrane reactor, due to selective permeation of hydrogen from reaction zone to permeate side enables us to increase the conversion by shifting the thermodynamic equilibrium to the right. Further with increasing temperature, H_2-flux in Pd-MPSS membrane increase which is reflected in increased conversion by equilibrium shift. Our experimental SMR study in Pd-MPSS membrane reactor confirmed this enhanced methanol conversions.

The effect of steam to methanol feed ratio (S/M, mol/mol) on hydrogen recovery in the membrane reactor is shown in Figure 29 for a temperature range of 200^{o}C to 300^{o}C. Hydrogen recovery was defined as the fractional recovery of hydrogen in the permeate side to theoretical hydrogen production for a given methanol conversion in the reaction zone. For a given steam to methanol feed ratio, hydrogen recovery increases with temperature. However, for a given temperature the hydrogen recovery decreases with increased S/M ratio. This decrease in recovery can be attributed to dilution in the reaction zone by excess water vapor (steam). There are some deviations in the model prediction of the hydrogen recovery; however the model predicted the experimental trend. The increase in hydrogen recovery with temperature can be attributed to reaction rates and hydrogen permeability, both of which increases with temperature.

In SMR, steam to methanol ratio has minimal effect on methanol conversion as shown in Figure 30 for three temperatures. As expected, with increased temperature one would expect higher conversion for endothermic reactions. With increased S/M ratio, steam acts as diluents and may contribute in slight reduction in the methanol conversion. The membrane reactor model predicted this trend as shown in Figure 30.

The selectivity of carbon monoxide and hydrogen as function of steam to methanol feed ratio in Pd-MPSS membrane reactor for SRM is shown in Figure 31 for three temperatures (200^{o}C, 250^{o}C and 300^{o}C). We defined the selectivity as % molar ratio of a component to sum of all product components. The results show that the S/M ratio is insensitive of H_2-selectivity and almost independent of temperature. However, CO-selectivity is very sensitive to temperature. Since the water-gas shift reaction is exothermic, this behavior is expected due decreased reaction rate at higher temperature. It appears from this limited data that S/M ratio may have some effect on CO-selectivity and there may be an optimum S/M ratio for maximum CO-selectivity for a given reaction temperature. This needs to be validated by further study.

The SMR reaction was carried out Pd-MPSS membrane over a period of thirty six hour in on/off mode. At the end of the experiment, we looked at the surface morphology of the used membrane by SEM analysis. In Figure 32, we present the SEM images of a freshly prepared Pd-MPSS membrane and the membrane exposed to SRM reactions. It is clear that during the SRM reactions over time, the membrane microstructure deteriorated significantly. Carbon soot deposition is visible with Pd-film peeling and/or pitting. The change in Pd-film structure may be attributed to hydrogen embrittlement as the SRM reactions were carried out at or below 300^{o}C.

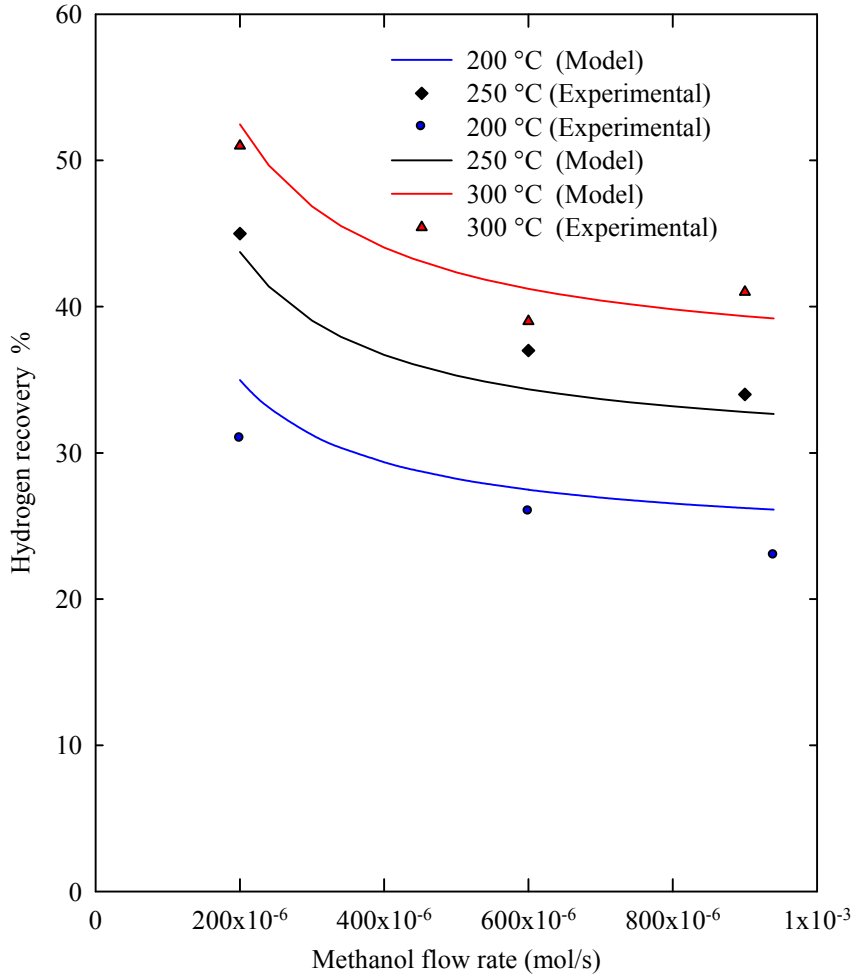

Figure 29. Effect of methanol flow rate on hydrogen recovery in membrane reactor (operating conditions: steam to methanol ratio (S/M) = 1, reactor side pressure = 50 psi, permeate side pressure =14.7 psi, and catalyst loading = 5.56 gm).

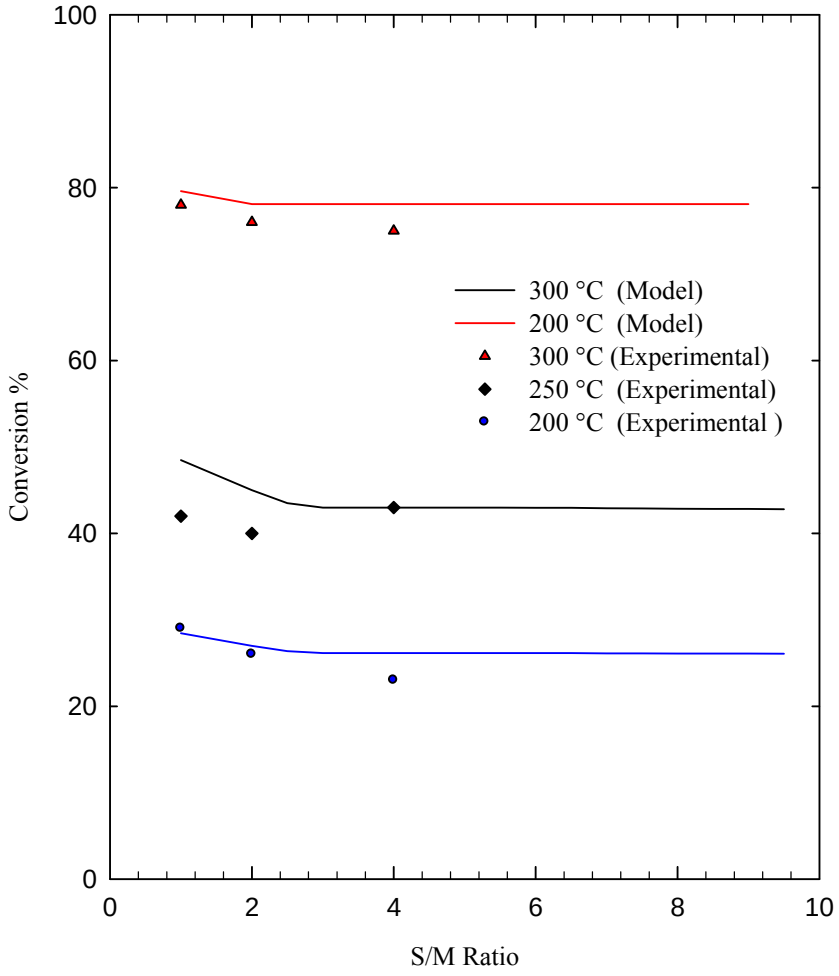

Figure 30. Effect of S/M ratio on methanol conversion in membrane reactor (operating conditions: catalyst time factor = 9.5, reactor side pressure = 50 psi, permeate side pressure = 14.7 psi, and catalyst loading = 5.56 gm).

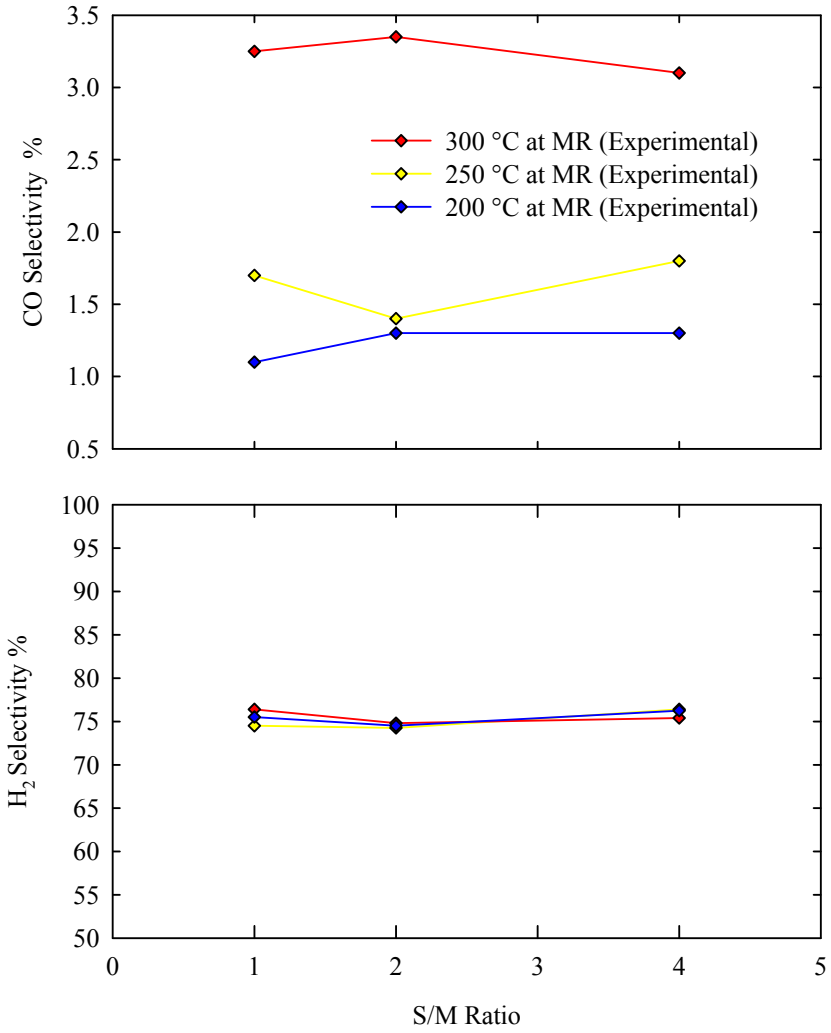

Figure 31. Effect of S/M ratio on CO and H_2 selectivity in membrane reactor (operating conditions: catalyst time factor = 9.5, reactor side pressure = 50 psi, permeate side pressure = 14.7 psi, and catalyst loading = 5.56 gm).

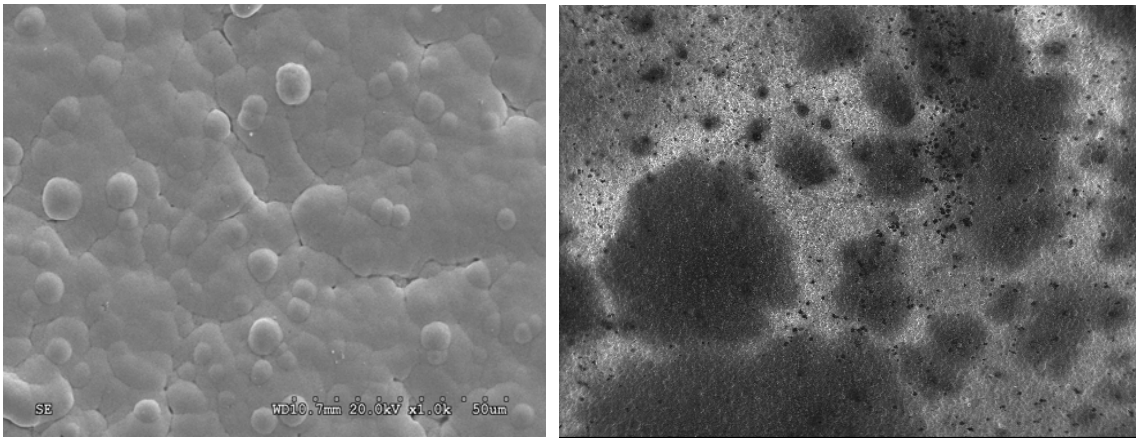

(a) (b)

Figure 32. Typical SEM micrographs showing (a) freshly prepared membrane microstructures, and (b) membrane microstructure after subjected to heat treatment and long term reactor applications.

CONCLUSIONS

Conventional electroless plating (CEP) process is greatly limited by the formation of dendritic structures throughout the target surface that result non uniformity in deposition morphology and microstructure. In this work, we focused on further improving the Pd-deposition morphology and grain structure by revisiting the sensitization and activation steps and electroless plating process. The findings of this work are summarized as follows:

- The morphology of the Pd-film deposition in elctroless plating strongly depends on the substrate sensitization and activation step. The micro-bubbles that evolve during electroless plating play a significant role on microstructure of the deposited film. We showed that the Pd-grain growth and grain microstructure can be controlled and manipulated by adding surface active agents in the electroless plating process. Of anionic, cationic and non-ionic surfactants, cationic surfactant was found to be most effective in controlling micro-bubbles at solid-gas-liquid interfaces. Pd-MPSS membrane fabricated in presence of cationic surfactant (DTAB) showed excellent Pd-grain formation and agglomeration, resulting membrane showed excellent H_2-permselectivity.
- Pulsed Laser Deposition (PLD) can be used to activate MPSS substrate by depositing Pd-seeds instead of conventional $SnCl_2/PdCl_2$ sensitization and activation step. The resulting membrane fabricated by electroless plating was found to be extremely thin, where H_2-transport is governed by surface diffusion which is different from activated solution-diffusion transport as commonly observed in thicker Pd-film. As an activation step, PLD was found to be very effective; however for large-scale membrane development current PLD technology is inadequate. Consequently, we did not further explore PLD for MPSS substrate activation.
- Pd-MPSS membrane fabricated by DTAB induced electroless plating method was tested in membrane-reactor configuration to study SMR and we demonstrated that the membrane-reactor can provide higher conversion and yield of hydrogen by equilibrium shift compared to conventional packed-bed reactor. SMR membrane reactor model accurately predicted the reactor performance trend.

The poor control on Pd-grain size distribution and non-uniform film deposition are major impediments to successful use of electroless plating as method for fabrication of defect-free Pd-composite membrane. In this research, we addressed this challenge by developing a novel; surfactant induced electroless plating (SIEP) and fabricated defect-free Pd-MPSS membrane. We believe that this is a significant development in Pd-MPSS membrane fabrication by electroless plating. This work resulted in a US patent application [35].

FUTURE WORK

Based on our success in fabrication of defect-free Pd-MPSS composite membrane by SIEP, we will continue our work to further develop the SIEP for fabrication of Pd-alloy MPSS composite membranes for high temperature, high pressure H_2-separtion and membrane reactor-separation applications. A short list of future work includes:

- Develop processing technology for the deposition of continuous, thin, integral, stable films of Pd-alloy (Pd-Ag, and Pd-Cu) on MPSS planar substrate by surfactant induced electroless plating (SIEP).

- Demonstrate the application of Pd-alloy-MPSS membranes in membrane reactor using steam methane reforming (SMR) and steam reforming of methanol as example reaction systems for simultaneous production and separation of hydrogen by equilibrium shift.

ACKNOWLEDGMENTS

This research was sponsored by the U.S. Department of Energy – HBCU Program, under Award No. DE-FG26-05NT42492. Dr. Arun Bose, NETL, Pittsburgh, is the DOE Project Officer. However, any opinions, findings, and conclusions or recommendations expressed herein are those of the author and do not necessarily reflect the views of the DOE. Analytical support from the Center for Advanced Materials and Smart Structures (CAMSS) of North Carolina A&T State University is gratefully acknowledged with special thanks to Drs. Jag Sankar, D. Kumar and Zhigang Xu.

REFERENCES

1. "National Hydrogen Energy Road Map," Based on the results of National Hydrogen Energy Road Map Workshop, Washington, DC, April 2-3, 2002, US DOE (Nov 2002).
2. "A National Vision of America's Transition to A Hydrogen Economy – To 2030 and Beyond," Based on the results of National Hydrogen Vision Meeting, Washington, DC, November 15-16, 2001, US DOE (February 2002).
3. Paglieri, S. (1999). "Palladium and palladium-cupper composite membranes for hydrogen separation." *PhD. Dissertation*, Colorado School of Mines, Golden, CO.
4. Collins, J.P., and J.D. Way (1993). *Ind. Eng. Chem. Res.,* **32**, 3006-3013.
5. Hsiesh, P.H. (1996). Inorganic Membrane for Separation and Reaction, Elsevier, New York, NY.
6. Souleimanova, R.S., M.A. Mukasyan, and A. Varma (2001). *Separation and Purification Technology,* **25**(1-3), 79-86.
7. Souleimanova, R. S., A. S. Mukasyan, and A. Varma (2002). *AIChE Journal,* **48**(2), 262-268.
8. Tong, J., R. Shirai, Y. Kashima, and Y. Matsumura (2005). *J. Membr. Sci*., **260**, 84.
9. Shu, J., B.P.A. Grandjean, A. van Neste, and S. Kaliaguine (1991). *Can. J. Chem. Eng.*, **69**, 1036-1060.
10. Ma Y.H., I.P. Mardilovich, and E.E. Engwall (2003). *Annal New York Academy of Science,* **984**, 346.
11. Lu, G.Q., J.C. Diniz da Costa, M. Duke, R. Socolow, R.H. Williams, and T. Kreutz (2007). *J. Colloid and Interface Science*, **314**, 589-603.
12. Souleimanova, R.S., A.S. Mukasyan, and A. Varma (2000). *J. Memb. Sci.,* **166**, 249-257.
13. Roa, F., D. Way, R.L. McCormick, and S.N. Paglieri (2003). *Chemical Engineering Journal*, **93**, 11-22.

14. Goto, S., S. Assabumrungrat, T. Tagawa, and P. Prasethdam (2000). *J. Memb. Sci*., **175**, 19-24.

15. Hou, K., and R. Hughes (2002). *J. Memb. Sci.*, **206**, 119-130.

16. Rothenberger, K.S., A.V. Cugini, B.H. Howard, R.P. Killmeyer, M.V. Ciocco, B.D. Morreale, R.M. Enick, F. Bustamante, I.P. Mardilovich, and Y.H. Ma (2004). *J. Memb. Sci.,* **244**, 55-68.

17. Lee, D. W., Y.G. Lee, S.E. Nam, S.K. Ihm, and K.H. Lee (2003). *J. Memb. Sci.,* **220**, 137-153.

18. Mardilovich, P. P., Y. She, Y. H. Ma, and M.H. Rei (1998). *AIChE Journal*, **44** (2), 310.

19. "Metal Finishing – Guidebook and Directory" published by Metal and Plastics publications, Inc., 169 (1975).

20. Kawagoshi, S., Japanese Patent (Kokai Tokkyo Koho), 77,733 (1977).

21. Yeung, K.L., and A. Varma (1995). *AIChE J.,* **49**, 2131.

22. Wu, L.Q., N. Xu, and J. Shi (2000). *Ind. Eng. Chem. Res.,* **39**, 342.

23. Zao, H.B., K. Pflanz, J.H. Gu, A.W. Li, N. Stroh, H. Brunner, and G.X. Xiong (1998). *J. Membr. Sci.,* **142**, 147.

24. Yeung, K.L., S.C.Christansen, and A. Varma (1999). *J. Membr. Sci.,* **159**, 107

25. R.K. Singh, and D. Kumar (1998). *Materials Science and Engineering R* (Reports), R22, 113.

26. Santacesairia, E., and S. Carra (1983). *Appl. Catal*., **5**, 345-358.

27. Amphlett, J.C., M. J. Evans, R.F. Mann, and R.D. Weir (1985). *Can. J. Chem. Eng.,* **63,** 605-611.

28. Peppley B.A., J.C. Amphlett, L.M. Kearns, and R.F. Mann (1999). *Appl. Catal.: Gen*. **179**, 31-49.

29. Gallucci, F., L. Paturzo, and A. Basile, (2004). *Ind. Eng. Chem. Res,*. **43**, 2420-2432.

30. Basile, A., S. Tosti, G. Capannelli, G. Vitulli, A. Iulianelli, F. Gallucci, and E. Drioli, (2006). *Catal. Today,* **118**, 237-245.

31. Basile, A., F. Gallucci, and L. Paturzo (2005). *Catal. Today,* **104**, 244-250.

32. Gallucci, F., and A. Basile (2006). *Intl. J. Hydrogen Energy,* **31**, 2243-2249.

33. Gallucci, F., A. Basile, and E. Drioli (2007). *Sep. & Purific. Rev.,* **36** (2), 175-202.

34. Akanda, M.H., (2007). "Modeling of Methanol-Steam Reforming in a Pd-Based. Membrane Reactor," MS Thesis, North Carolina A&T State University, Greensboro, NC.

35. Ilias, S., and M.A. Islam, "Method for preparing thin films by electroless plating," U.S. Patent Application No. 61052798 (May 2008) - Pending